Cerema

Direction territoriale Est
Laboratoire Régional de Strasbourg

L'expertise technique au service de l'État
et des collectivités

Utilisation de l'équation de transport pour la prévision du bruit

Vers un nouveau modèle d'acoustique du bâtiment

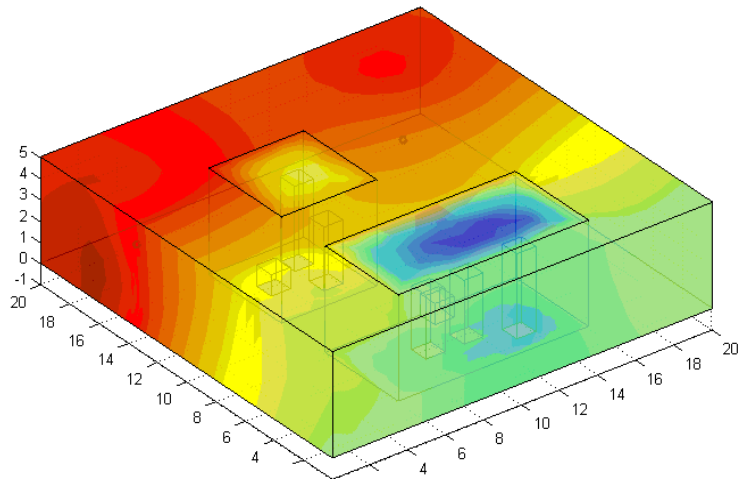

Mai 2014

Direction territoriale Est

Cédric FOY

PhD Acoustics
Researcher in Building Acoustics - Acoustics Group

Tél : 03 88 77 79 26 - Fax : 03 88 77 46 20
cedric.foy@cerema.fr

Center for expertise and engineering on risks,
urban and country planning, environment and mobility - www.cerema.fr
Régional Laboratory of Strasbourg - 11, rue Jean Mentelin
BP 9 - 67035 Strasbourg Cedex 2 - France - Phone : +33 (0)3 88 77 46 00

Références de la commande

Sans objet

Référence du dossier

Numéro de dossier : 2013-76-025 OPALHA2
Numéro de référence du service documentation : sans objet
Objet : Exercices destinés aux étudiants de l'Université de Strasbourg – IRMA Institut de Recherche Mathématique Avancée, UMR 7501

Historique des versions du document

Version	Auteur	Commentaires
1	Cédric Foy	

Affaire suivie par

Cédric Foy – Chargé de Recherche en Acoustique du Bâtiment
Tél : 03.88.77.79.26 / Fax : 03.88.77.46.20
Mail : cedric,foy@cerema.fr

Chapitre 1

Présentation

1.1 Contexte

Face au défi du réchauffement climatique, le Grenelle de l'Environnement a mis en exergue la nécessité d'améliorer significativement les performances thermiques des bâtiments d'habitation. Il maintenant bien connu1 qu'une action de réhabilitation thermique peut dégrader les performances acoustiques d'un bâtiment. Or le bruit demeure l'une des nuisances qui préoccupent le plus les français. La réhabilitation thermique ne peut donc se faire au détriment de l'acoustique. En parallèle à ces projets de réhabilitation, la ministre du logement a présenté, mercredi 2 octobre 2013, en conseil des ministres trois ordonnances2 visant à faciliter la réalisation d'opérations d'aménagement pour construire davantage de logements. Ces nouveaux bâtiments, désormais plus performants thermiquement, doivent aussi être garants de performances minimales en terme d'isolation acoustique (arrêté du 30 juin 1999) et qui peuvent aussi être renforcées par prescription du maître d'ouvrage soucieux d'une démarche HQE3 élevée. Côté Direction de l'Habitat, de l'Urbanisme et des Paysages (DHUP), l'importance de prendre en compte l'acoustique au sein des bâtiments a également été soulignée par l'apparition quasi-simultanée de deux guides4, l'un à destination des contrôleurs de l'État, l'autre ciblant les maîtres d'ouvrages en vue de les responsabiliser.

En parallèle aux problématiques de logements doit s'ajouter celles relatives aux bâtiments tertiaires comme les ERP, établissement recevant du public. Les arrêtés du 25 avril 2003 relatifs à fixent notamment les performances acoustiques à atteindre dans le cas des établissements de santé, d'enseignement et dans les hôtels. En sus de l'étude des performances acoustiques (isolation acoustique), s'ajoute ici celle de la caractérisation du champ sonore de ces bâtiments. L'objectif de caractériser le champ sonore est alors lié à une notion de confort, d'urgence, de santé... : comment un professeur peut-il enseigner dans une salle trop réverbérante ? Quels sont les risques encourus par un patient lorsque l'acoustique de la salle d'opération gêne le chirurgien ? Quelle est la conséquence d'une procédure d'évacuation d'urgence mal perçue au sein d'un hall de gare ou d'une station de métro ?

Malheureusement, côté approche de prévision acoustique, soit les modèles utilisés de calcul des performances et de caractérisation acoustiques s'appuient sur des hypothèses liés à la théorie de Sabine du siècle et sont donc valables uniquement pour des locaux de dimensions homogènes d'absorption faible et uniforme, soit ces modèles reposent sur des approches statistiques gonflant les temps de calcul dans le cas des locaux tertiaires souvent de grandes dimensions ou dans le cas de bâtiments de forme complexe (réseaux de salles reliées entre elles par des ouvertures, open-spaces tels que les plateformes téléphoniques, cuisines ouvertes sur séjours...).

1.2 Le modèle proposé

Cependant, depuis plusieurs années, un modèle a récemment été proposé. Il s'agit d'un « modèle de transport », qui a été développé dans le cadre d'une collaboration entre l'IFSTTAR (laboratoire LAE), l'Université de La Rochelle (laboratoire Lasie) et l'Université de Poitiers (laboratoire Pprime). Ce travail a donné lieu à de nombreuses publications, thèses, rapports...par les différents partenaires du projet. En outre, il a été démontré sa capacité à intégrer les principaux phénomènes acoustiques (réverbération, transmission...) et à modéliser la propagation des champs sonores réverbérés au sein de bâtiments de forme complexe.

Depuis le 27 novembre 2012, un projet ADEME réunissant les mêmes partenaires (CEREMA/Ifsttar/Univ. La Rochelle/Univ. Poitiers) existe. Le travail proposé porte sur le développement d'un code de calcul pour des applications de recherche et des études opérationnelles, destiné à la prévision de l'acoustique architecturale. L'approche proposée par le modèle de transport offre aussi l'avantage de pouvoir traiter simultanément l'acoustique urbaine et l'acoustique du bâtiment, et donc en particulier, le couplage entre le milieu intérieur et le milieu extérieur. Ce projet comporte trois volets principaux :

- la résolution de plusieurs verrous scientifiques (diffraction, lois de réflexion mixtes, diffusion du son en milieu urbain...) ;
- la réalisation d'un code de résolution spécifiquement adapté aux besoins acoustiques ;
- la poursuite du développement de l'interface multi-codes I-Simpa développé par Ifsttar (accueillant le code de calcul du modèle de transport) et du logiciel de tir de particules SPPS (logiciel de référence pour la validation du modèle de transport).

A terme, l'ensemble de ce travail sera valorisé par la mise à disposition d'un outil auprès de l'ensemble de la communauté scientifique et technique (publique ou privée). A ce titre, une réflexion « libre (publique) /payant (privée) »sera menée en prenant contact avec des personnalités du monde de la recherche et académique, et des éditeurs/diffuseurs de logiciels reconnus en France.

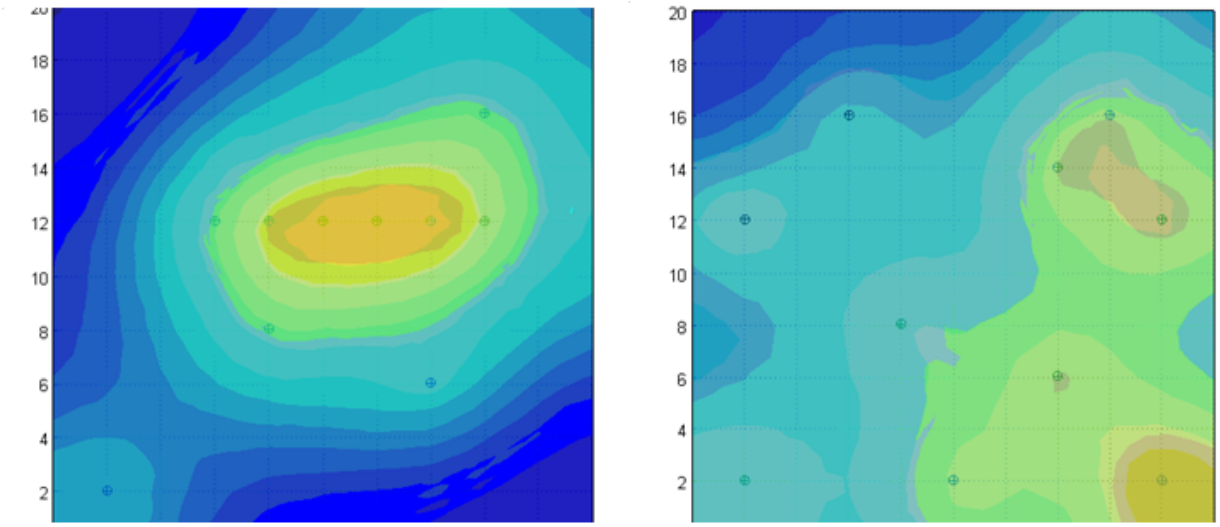

FIGURE 1.1 – Exemple : utilisation du modèle dans le choix du positionnement de sources industrielles au sein d'un atelier.

Chapitre 2

Présentation du modèle de transport

2.1 Introduction

Le modèle proposé repose sur une équation de transport et a pour objectif de modéliser le champ sonore d'un local de volume V et de surface de ses parois S. Il s'appuie sur l'idée que ce champ est composé de particules sonores se propageant dans toutes les directions avec une vitesse identique (norme).

2.2 Présentation du modèle

Le modèle est exprimé ici pour les particules sonores de direction de propagation θ, ϕ pendant le temps dt. Pour avoir le champ sonore dans sa globalité, il faut bien sûr intégrer sur l'ensemble des directions de propagation.

2.2.1 Equation volumique

Le système d'équations proposé est composé respectivement d'une équation volumique modélisant les phénomènes acoustiques au sein du volume de la salle d'étude :

$$\frac{\partial w(\vec{r},\theta,\phi,t)}{\partial t} = -\vec{v}\cdot\vec{\nabla}w(\vec{r},\theta,\phi,t)) - Mvw(\vec{r},\theta,\phi,t) + w_{sce}(\vec{r},\theta,\phi,t)) \quad \vec{r}\in dV. \tag{2.1}$$

La grandeur $w(\vec{r},\theta,\phi,t)$ correspond à la densité d'énergie acoustique, elle est en $Wm^{-3}s$. Le terme $\vec{v}$ est la vitesse de propagation des particules (vitesse du son), (θ,ϕ) donnant la direction de propagation.

Le premier terme du second membre correspond au nombre de particules sonores entrant ou sortant au sein de l'élément de volume dV sans avoir subi de modification au niveau de leur direction. Le second terme correspond au nombre de particules sonores ayant été absorbées du fait du phénomène d'atténuation atmosphérique. Le terme M est un coefficient d'atténuation atmosphérique que nous choisirons ici constant. Le dernier terme correspond à une densité d'énergie acoustique amenée par une source sonore.

Cette équation traduit deux phénomènes de propagation :

- si $\vec{v}\cdot\vec{\nabla}[.] > 0$, alors $\frac{\partial}{\partial t}[.]$ est négatif signifiant que, en un point donné le nombre de particules diminue avec le temps. Le gradient est ici de sens identique à la direction de propagation des particules signifiant un phénomène de dispersion.
- si $\vec{v}\cdot\vec{\nabla}[.] < 0$, alors $\frac{\partial}{\partial t}[.]$ est positif signifiant que, en un point donné le nombre de particules augmente avec le temps. Le gradient est ici de sens contraire à la direction de propagation des particules signifiant un phénomène de concentration.

2.2.2 Conditions aux limites

Les jeux d'équations suivants correspondent à deux conditions aux limites sur la surface S de la salle avec $\vec{n}$ la normale extérieure à celle-ci.

Une première condition aux limites correspond finalement à l'expression de l'énergie absorbée au niveau de la paroi :

$$\begin{cases} (dE_{abs}(\vec{r},\theta,\phi,t) =)\vec{v}\cdot\vec{n}w(\vec{r},\theta,\phi,t) = \alpha\,(1-d)\times 1\times\hat{\vec{v}}\cdot\vec{n}\times w(\vec{r},\hat{\theta},\hat{\phi},t) \\ +\int_0^{2\pi}\int_0^{\frac{\pi}{2}} \alpha d\times\frac{1}{\pi}\frac{\vec{v}}{v}\cdot\vec{n}\times\vec{v}^{\,'}\cdot\vec{n}\times w(\vec{r},\theta^{'},\phi^{'},t)\sin\theta^{'}d\theta^{'}d\phi^{'} \quad \vec{v}\cdot\vec{n}>0,\hat{\vec{v}}\cdot\vec{n}>0,\vec{v}^{\,'}\cdot\vec{n}>0,\vec{r}\in dS \\ (dE_{abs}(\vec{r},\theta,\phi,t) =)\vec{v}\cdot\vec{n}w(\vec{r},\theta,\phi,t) = 0 \quad \vec{v}\cdot\vec{n}<0,\vec{r}\in dS. \end{cases} \tag{2.2}$$

Une seconde condition aux limites correspond finalement à l'expression de l'énergie réfléchie au niveau de la paroi :

$$\begin{cases} (dE_{ref}(\vec{r},\theta,\phi,t) =)\vec{v}\cdot\vec{n}w(\vec{r},\theta,\phi,t) = R\,(1-d)\times 1\times\hat{\vec{v}}\cdot\vec{n}\times w(\vec{r},\hat{\theta},\hat{\phi},t) \\ +\int_0^{2\pi}\int_0^{\frac{\pi}{2}} Rd\times\frac{1}{\pi}\frac{\vec{v}}{v}\cdot\vec{n}\times\vec{v}^{\,'}\cdot\vec{n}\times w(\vec{r},\theta^{'},\phi^{'},t)\sin\theta^{'}d\theta^{'}d\phi^{'} \quad \vec{v}\cdot\vec{n}<0,\hat{\vec{v}}\cdot\vec{n}>0,\vec{v}^{\,'}\cdot\vec{n}>0,\vec{r}\in dS \\ (dE_{ref}(\vec{r},\theta,\phi,t) =)\vec{v}\cdot\vec{n}w(\vec{r},\theta,\phi,t) = 0 \quad \vec{v}\cdot\vec{n}>0,\vec{r}\in dS. \end{cases} \tag{2.3}$$

Par définition, nous avons :

$$\alpha + R = 1, \tag{2.4}$$

où α et R sont respectivement le coefficient d'absorption et le coefficient de réflexion, compris entre 0 et 1.

De façon à être au plus proche de l'acoustique des salles, nous avons ici distingué ici les directions de propagation $\vec{v}$ entre elles. Nous définissons la direction de propagation $\vec{v} = \hat{\vec{v}}$ telle que $\hat{\vec{v}}\cdot\vec{n} = -\vec{v}\cdot\vec{n}$, correspondant à une « réflexion spéculaire », et les autres directions de propagation $\vec{v} = \vec{v}^{\,'}$ telle que $\vec{v}^{\,'}\cdot\vec{n} \neq -\vec{v}^{\,'}\cdot\vec{n}$, correspondant à une « réflexion non spéculaire ».

Nous avons ici introduit les termes suivants :

- $P(\textit{spéculaire}) = 1-d$: probabilité que le type de réflexion soit spéculaire, c'est à dire que $\vec{v} = \hat{\vec{v}}$,
- $P(\vec{v},\vec{v}\mid \textit{spéculaire}) = \delta_{\vec{v}\,,\,\hat{\vec{v}}}$: probabilité que la réflexion soit spéculaire sachant que la direction d'incidence est $\vec{v}$ et que la direction de « réflexion »est $\vec{v}$,
- $P(\textit{non spéculaire}) = d$: probabilité que le type de réflexion soit non spéculaire, c'est à dire que $\vec{v} = \vec{v}^{\,'}$
- $P(\vec{v},\vec{v}\mid \textit{non spéculaire}) = \frac{1}{\pi}\frac{\vec{v}}{v}\cdot\vec{n}$: probabilité que la réflexion soit non spéculaire sachant que la direction d'incidence est $\vec{v}$ et que la direction de « réflexion »est $\vec{v}$.

Le terme d introduit ici (coefficient de diffusivité des parois), est un coefficient constant compris entre 0 et 1.

2.3 Autres grandeurs

L'intensité acoustique $I(\vec{r},\vec{v},t)$ (en $\left[Wm^{-2}\right]$) est la puissance transportée par les ondes sonores dans une direction de propagation $\vec{v}$ donnée, par unité de surface dS perpendiculairement à cette direction. L'intensité acoustique s'écrit en fonction de la densité d'énergie acoustique $w(\vec{r},\vec{v},t)$ de la façon suivante :

$$I(\vec{r},\vec{v},t) \propto \vec{v}\cdot\vec{n}w(\vec{r},\vec{v},t), \tag{2.5}$$

où $\vec{n}$ est la normale (souvent extérieure si la surface est fermée) à la surface S. La puissance acoustique $W(\vec{r},\vec{v},t)$ peut être vue comme l'intensité traversant une surface S. Elle s'exprime en $[W]$ et s'écrit alors en fonction de la densité d'énergie de la façon suivante :

$$W(\vec{r},\vec{v},t) \propto \vec{v}\cdot\vec{n}w(\vec{r},\vec{p},t)\times S, \tag{2.6}$$

où bien, elle peut être vue comme la variation au cours du temps de la densité d'énergie acoustique au sein d'un volume V, soit :

$$W(\vec{r},\vec{v},t) \propto \frac{dw(\vec{r},\vec{v},t)}{dt} \times V. \tag{2.7}$$

Enfin, l'énergie acoustique $E(\vec{r},\vec{v},t)$ est le produit de la puissance acoustique par le temps et s'exprime en $[W.s]$, soit :

$$E(\vec{r},\vec{v},t) \propto \vec{v} \cdot \vec{n}w(\vec{r},\vec{v},t) \times S \times t, \tag{2.8}$$

où bien :

$$E(\vec{r},\vec{v},t) \propto w(\vec{r},\vec{v},t) \times V. \tag{2.9}$$

Chapitre 3

Modèle proposé et théorie de la réverbération

3.1 introduction

Nous donnons ici le développement basé sur le modèle proposé et permettant de retrouver la loi de décroissance de la densité d'énergie bien connue en théorie de la réverbération. Cette théorie s'appuie sur l'idée champ sonore dit « diffus », c'est à dire d'un champ sonore identique en tous points de l'espace et en toutes directions.

3.2 Développement

Le système d'équations proposé est rappelé ici :

$$\frac{\partial w(\vec{r},\theta,\phi,t)}{\partial t} = -\vec{v}\cdot\vec{\nabla}w(\vec{r},\theta,\phi,t)) - Mvw(\vec{r},\theta,\phi,t) + w_{sce}(\vec{r},\theta,\phi,t) \quad \vec{r}\in dV, \tag{3.1}$$

$$\begin{cases} (dE_{abs}(\vec{r},\theta,\phi,t) =)\vec{v}\cdot\vec{n}w(\vec{r},\theta,\phi,t) = \alpha\,(1-d)\,\hat{\vec{v}}\cdot\vec{n}w(\vec{r},\hat{\theta},\hat{\phi},t) \\ +\int_0^{2\pi}\int_0^{\frac{\pi}{2}} \alpha d\frac{1}{\pi}\frac{\vec{v}}{v}\cdot\vec{n}\vec{v}^{\,'}\cdot\vec{n}w(\vec{r},\theta^{'},\phi^{'},t)\sin\theta^{'}d\theta^{'}d\phi^{'} \quad \vec{v}\cdot\vec{n}>0,\hat{\vec{v}}\cdot\vec{n}>0,\vec{v}^{\,'}\cdot\vec{n}>0,\vec{r}\in dS \\ (dE_{abs}(\vec{r},\theta,\phi,t) =)\vec{v}\cdot\vec{n}w(\vec{r},\theta,\phi,t) = 0 \quad \vec{v}\cdot\vec{n}<0,\vec{r}\in dS. \end{cases} \tag{3.2}$$

Il est donc composé de la première condition aux limites (équation 2.2).
Le premier terme du second membre peut s'écrire :

$$\vec{v}\cdot\vec{\nabla}w(\vec{r},\theta,\phi,t)) = \vec{\nabla}\left[\vec{v}w(\vec{r},\theta,\phi,t))\right] - w(\vec{r},\theta,\phi,t))\cdot\vec{\nabla}\left[\vec{v}\right]. \tag{3.3}$$

Comme la direction de propagation $\vec{v}$ et la normale $\vec{n}$ ne dépendent pas de l'espace, il reste seulement :

$$\vec{v}\cdot\vec{\nabla}w(\vec{r},\theta,\phi,t)) = \vec{\nabla}\left[\vec{v}w(\vec{r},\theta,\phi,t))\right]. \tag{3.4}$$

En remplaçant au sein de l'équation 3.1 et en faisant l'opération $\int_{-\frac{L_z}{2}}^{\frac{L_z}{2}}\int_{-\frac{L_y}{2}}^{\frac{L_y}{2}}\int_{-\frac{L_x}{2}}^{\frac{L_x}{2}}(.)dxdydz$, nous obte-

nons :

$$\begin{aligned}\int_{-\frac{L_z}{2}}^{\frac{L_z}{2}}\int_{-\frac{L_y}{2}}^{\frac{L_y}{2}}\int_{-\frac{L_x}{2}}^{\frac{L_x}{2}}\frac{\partial w(\vec{r},\theta,\phi,t)}{\partial t}dxdydz &= -\int_{-\frac{L_z}{2}}^{\frac{L_z}{2}}\int_{-\frac{L_y}{2}}^{\frac{L_y}{2}}\int_{-\frac{L_x}{2}}^{\frac{L_x}{2}}\vec{\nabla}\left[\vec{v}w(\vec{r},\theta,\phi,t))\right]dxdydz \\ -\int_{-\frac{L_z}{2}}^{\frac{L_z}{2}}\int_{-\frac{L_y}{2}}^{\frac{L_y}{2}}\int_{-\frac{L_x}{2}}^{\frac{L_x}{2}}\left[Mvw(\vec{r},\theta,\phi,t)\right]dxdydz &+ \int_{-\frac{L_z}{2}}^{\frac{L_z}{2}}\int_{-\frac{L_y}{2}}^{\frac{L_y}{2}}\int_{-\frac{L_x}{2}}^{\frac{L_x}{2}}w_{sce}(\vec{r},\theta,\phi,t)dxdydz\end{aligned} \tag{3.5}$$

A l'aide du théorème de la divergence :

$$\oiint_S \vec{F}\cdot\vec{n}dS = \iiint \vec{\nabla}\cdot\vec{F}dV, \tag{3.6}$$

nous pouvons remplacer la première intégrale du second membre, nous obtenons :

$$\begin{aligned}\int_{-\frac{L_z}{2}}^{\frac{L_z}{2}}\int_{-\frac{L_y}{2}}^{\frac{L_y}{2}}\int_{-\frac{L_x}{2}}^{\frac{L_x}{2}}\frac{\partial w(\vec{r},\theta,\phi,t)}{\partial t}dxdydz &= -\oiint_S \vec{v}\cdot\vec{n}w(\vec{r},\theta,\phi,t))dS \\ -\int_{-\frac{L_z}{2}}^{\frac{L_z}{2}}\int_{-\frac{L_y}{2}}^{\frac{L_y}{2}}\int_{-\frac{L_x}{2}}^{\frac{L_x}{2}}\left[Mvw(\vec{r},\theta,\phi,t)\right]dxdydz &+ \int_{-\frac{L_z}{2}}^{\frac{L_z}{2}}\int_{-\frac{L_y}{2}}^{\frac{L_y}{2}}\int_{-\frac{L_x}{2}}^{\frac{L_x}{2}}w_{sce}(\vec{r},\theta,\phi,t)dxdydz\end{aligned} \tag{3.7}$$

Comme il a été vu, il faut intégrer aussi sur l'ensemble des directions, comme la condition aux limites est nulle lorsque $\vec{v}\cdot\vec{n} < 0$, nous avons l'équation suivante :

$$\begin{aligned}\int_0^{2\pi}\int_0^{\pi}\left[\int_{-\frac{L_z}{2}}^{\frac{L_z}{2}}\int_{-\frac{L_y}{2}}^{\frac{L_y}{2}}\int_{-\frac{L_x}{2}}^{\frac{L_x}{2}}\frac{\partial w(\vec{r},\theta,\phi,t)}{\partial t}dxdydz\right]\sin\theta d\theta d\phi &= \\ -\int_0^{2\pi}\int_0^{\frac{\pi}{2}}\left[\oiint_S \vec{v}\cdot\vec{n}w(\vec{r},\theta,\phi,t))dS\right]\sin\theta d\theta d\phi & \\ -\int_0^{2\pi}\int_0^{\pi}\left[\int_{-\frac{L_z}{2}}^{\frac{L_z}{2}}\int_{-\frac{L_y}{2}}^{\frac{L_y}{2}}\int_{-\frac{L_x}{2}}^{\frac{L_x}{2}}\left[Mvw(\vec{r},\theta,\phi,t)\right]dxdydz\right]\sin\theta d\theta d\phi & \\ +\int_0^{2\pi}\int_0^{\pi}\left[\int_{-\frac{L_z}{2}}^{\frac{L_z}{2}}\int_{-\frac{L_y}{2}}^{\frac{L_y}{2}}\int_{-\frac{L_x}{2}}^{\frac{L_x}{2}}w_{sce}(\vec{r},\theta,\phi,t)dxdydz\right]\sin\theta d\theta d\phi &\end{aligned} \tag{3.8}$$

Il est à noter que l'intégration sur θ est logiquement comprise entre 0 et π pour les termes volumiques et entre 0 et $\pi/2$ pour les termes surfaciques. En faisant maintenant l'opération $\oiint_S(.)dS$ sur l'équation 2.2, nous obtenons :

$$\begin{aligned}\oiint_S \vec{p}\cdot\vec{n}w(\vec{r},\theta,\phi,t)dS &= \\ +\oiint_S \alpha\left(1-d\right)\hat{\vec{v}}\cdot\vec{n}w(\vec{r},\hat{\theta},\hat{\phi},t)dS & \\ +\oiint_S\left[\int_0^{2\pi}\int_0^{\frac{\pi}{2}}\alpha d\frac{1}{\pi}\frac{\vec{v}}{v}\cdot\vec{n}\vec{v}^{\,'}\cdot\vec{n}w(\vec{r},\theta^{'},\phi^{'},t)\sin\theta^{'}d\theta^{'}d\phi^{'}\right]dS\ \vec{r}\in dS. &\end{aligned} \tag{3.9}$$

Le premier terme du second membre de l'équation 3.7 peut alors être rempacé par cette expression et nous obtenons :

$$\begin{aligned}
&\iint_{0\,0}^{2\pi\pi}\left[\int_{-\frac{L_z}{2}}^{\frac{L_z}{2}}\int_{-\frac{L_y}{2}}^{\frac{L_y}{2}}\int_{-\frac{L_x}{2}}^{\frac{L_x}{2}}\frac{\partial w(\vec{r},\theta,\phi,t)}{\partial t}dxdydz\right]\sin\theta d\theta d\phi = \\
&\qquad -\iint_{0\,0}^{2\pi\,\frac{\pi}{2}}\left[\oiint_S \alpha\,(1-d)\,\hat{\vec{p}}\cdot\vec{n}w(\vec{r},\hat{\theta},\hat{\phi},t)dS\right]\sin\theta d\theta d\phi \\
&-\iint_{0\,0}^{2\pi\,\frac{\pi}{2}}\left[\oiint_S\left[\iint_{0\,0}^{2\pi\,\frac{\pi}{2}}\alpha d\frac{1}{\pi}\frac{\vec{v}}{v}\cdot\vec{n}\vec{v}^{\,'}\cdot\vec{n}w(\vec{r},\theta^{'},\phi^{'},t)\sin\theta^{'}d\theta^{'}d\phi^{'}\right]dS\right]\sin\theta d\theta d\phi \\
&\qquad -\iint_{0\,0}^{2\pi\pi}\left[\int_{-\frac{L_z}{2}}^{\frac{L_z}{2}}\int_{-\frac{L_y}{2}}^{\frac{L_y}{2}}\int_{-\frac{L_x}{2}}^{\frac{L_x}{2}}\left[Mvw(\vec{r},\theta,\phi,t)\right]dxdydz\right]\sin\theta d\theta d\phi \\
&\qquad +\iint_{0\,0}^{2\pi\pi}\left[\int_{-\frac{L_z}{2}}^{\frac{L_z}{2}}\int_{-\frac{L_y}{2}}^{\frac{L_y}{2}}\int_{-\frac{L_x}{2}}^{\frac{L_x}{2}}w_{sce}(\vec{r},\theta,\phi,t)dxdydz\right]\sin\theta d\theta d\phi
\end{aligned} \tag{3.10}$$

Nous avons ainsi obtenu une équation générale incluant l'ensemble des phénomènes acoustiques (phénomènes surfaciques et volumiques) que nous écrivons sous la forme simplifiée suivante :

$$[A] = -\alpha\,(1-d)\,[B] - \frac{\alpha d}{\pi}[C] - [D] + [E], \tag{3.11}$$

en faisant ici l'hypothèse de coefficients d'absorption et de diffusivité constants.

En faisant l'hypothèse d'un champs réverbéré diffus, c'est à dire un champ réverbéré constant en tous points et en toutes directions, nous allons expliciter l'ensemble des termes.

Le terme $[A]$ s'écrit :

$$[A] = \iint_{0\,0}^{2\pi\pi}\left[\int_{-\frac{L_z}{2}}^{\frac{L_z}{2}}\int_{-\frac{L_y}{2}}^{\frac{L_y}{2}}\int_{-\frac{L_x}{2}}^{\frac{L_x}{2}}\frac{\partial w(\vec{r},\theta,\phi,t)}{\partial t}dxdydz\right]\sin\theta d\theta d\phi = 4\pi\times L_xL_yL_z\times\frac{\partial w(t)}{\partial t}. \tag{3.12}$$

De façon identique, le terme $[D]$ s'écrit :

$$[D] = \iint_{0\,0}^{2\pi\pi}\left[\int_{-\frac{L_z}{2}}^{\frac{L_z}{2}}\int_{-\frac{L_y}{2}}^{\frac{L_y}{2}}\int_{-\frac{L_x}{2}}^{\frac{L_x}{2}}\left[Mvw(\vec{r},\theta,\phi,t)\right]dxdydz\right]\sin\theta d\theta d\phi = 4\pi\times L_xL_yL_z\times M\frac{p}{m}w(t). \tag{3.13}$$

En supposant que la source sonore soit également indépendante de la position de l'espace et de la direction, le terme $[E]$ s'écrit :

$$[E] = \iint_{0\,0}^{2\pi\pi}\left[\int_{-\frac{L_z}{2}}^{\frac{L_z}{2}}\int_{-\frac{L_y}{2}}^{\frac{L_y}{2}}\int_{-\frac{L_x}{2}}^{\frac{L_x}{2}}w_{sce}(\vec{r},\theta,\phi,t)dxdydz\right]\sin\theta d\theta d\phi = 4\pi\times L_xL_yL_z\times w_{sce}(t). \tag{3.14}$$

Le terme $[B]$ s'écrit en tenant compte du fait que $\hat{\theta} = -\theta$ (réflexions spéculaires) et que $\hat{p} = p$:

$$\begin{aligned}[B] &= \int_0^{2\pi}\int_0^{\frac{\pi}{2}} \left[\oiint_S \hat{\vec{p}} \cdot \vec{n} w(\vec{r}, \hat{\theta}, \hat{\phi}, t) dS \right] \sin\theta d\theta d\phi \\ &= w(t) \oiint_S dS \int_0^{2\pi}\int_0^{\frac{\pi}{2}} \hat{v} \cos\hat{\theta} \sin\theta d\theta d\phi \\ &= w(t) \times 2 \times [L_x L_y + L_x L_z + L_y L_z] \times \pi v.\end{aligned} \tag{3.15}$$

Le terme $[C]$ peut être maintenant être modifié de la façon suivante :

$$\begin{aligned}[C] &= \int_0^{2\pi}\int_0^{\frac{\pi}{2}} \left[\oiint_S \left[\int_0^{2\pi}\int_0^{\frac{\pi}{2}} \frac{\vec{v}}{v} \cdot \vec{n}\vec{v}^{\,'} \cdot \vec{n} w(\vec{r}, \theta^{'}, \phi^{'}, t) \sin\theta^{'} d\theta^{'} d\phi^{'} \right] dS \right] \sin\theta d\theta d\phi \\ &= w(t) \oiint_S dS \int_0^{2\pi}\int_0^{\frac{\pi}{2}} \frac{\vec{v}}{v} \cdot \vec{n} \sin\theta d\theta d\phi \int_0^{2\pi}\int_0^{\frac{\pi}{2}} \vec{v}^{\,'} \cdot \vec{n} \sin\theta^{'} d\theta^{'} d\phi^{'} \\ &= w(t) \oiint_S dS \int_0^{2\pi}\int_0^{\frac{\pi}{2}} \cos\theta \sin\theta d\theta d\phi \int_0^{2\pi}\int_0^{\frac{\pi}{2}} v^{\,'} \cos\theta^{'} \sin\theta^{'} d\theta^{'} d\phi^{'} \\ &= w(t) \times 2 \times [L_x L_y + L_x L_z + L_y L_z] \times \pi^2 v\end{aligned} \tag{3.16}$$

Finalement, dans le cas d'un champ réverbéré diffus, nous avons l'équation suivante :

$$\begin{aligned}4\pi \times L_x L_y L_z \times \frac{\partial w(t)}{\partial t} = \\ -\alpha(1-d) \times 2\pi v w(t) \times [L_x L_y + L_x L_z + L_y L_z] - \alpha d \times 2\pi v w(t) \times [L_x L_y + L_x L_z + L_y L_z] \\ -4\pi \times L_x L_y L_z \times M v w(t) + 4\pi \times L_x L_y L_z \times w_{sce}(t)\end{aligned} \tag{3.17}$$

Nous obtenons :

$$\begin{aligned}4\pi \times L_x L_y L_z \times \frac{\partial w(t)}{\partial t} &= -\alpha \times 2\pi v w(t) \times [L_x L_y + L_x L_z + L_y L_z] \\ &-4\pi \times L_x L_y L_z \times M v w(t) + 4\pi \times L_x L_y L_z \times w_{sce}(t)\end{aligned} \tag{3.18}$$

soit :

$$\begin{aligned}L_x L_y L_z \times \frac{\partial w(t)}{\partial t} &= -\alpha \times \frac{v}{2} \times [L_x L_y + L_x L_z + L_y L_z] w(t) \\ &-L_x L_y L_z \times M v w(t) + L_x L_y L_z \times w_{sce}(t)\end{aligned} \tag{3.19}$$

soit :

$$w_{rev}(t) = w_{rev}(0) \exp - \left\{ \frac{\alpha v}{2} \left[\frac{1}{L_x} + \frac{1}{L_y} + \frac{1}{L_z} \right] + Mv \right\} t, \tag{3.20}$$

avec :

$$w_{rev}(0) = \frac{w_{sce}(0)}{\frac{\alpha v}{2} \left[\frac{1}{L_x} + \frac{1}{L_y} + \frac{1}{L_z} \right] + Mv}, \tag{3.21}$$

pour une source coupée à $t = 0$.

Nous retrouvons ici l'équation bien connue de la théorie de la réverbération donnée par Sabine.

Chapitre 4

Exercices proposés

4.1 Exercice 1

Le premier exercice proposé consiste à retrouver la loi de la décroissance de la théorie de la réverbération en partant cette fois de la seconde condition aux limites donnée en équation 2.3. Il s'agit donc d'établir une démonstration similaire à celle donnée au chapitre précédent.

La relation donnée en équation 2.4 sera sans doute utile.

4.2 Exercice 2

Comme il a été dit, le développement ci-dessus permet de retrouver une loi décroissance bien connue en faisant l'hypothèse que le champ sonore est diffus (champ sonore identique en tous points de l'espace et en toutes directions). Ce champ sonore est supposé être équivalent à un tel champ dès lors que l'absorption α est faible et dès lors que les dimensions du local sont homogènes entre elles (local de forme homogène).

I faut noter toutefois que dans le problème précédemment considéré, il existe une source sonore en tous points de l'espace. Dans la réalité, ceci n'est pas le cas, la source sonore est positionnée en un unique endroit $\vec{r} = \vec{r}_s$. L'objectif consisterait à retrouver la loi de décroissance d'un champ sonore diffus en réalisant un développement plus proche de la réalité.

Ceci nécessite sans doute l'utilisation d'une fonction de Green G. L'équation volumique du système proposé s'écrit alors par exemple :

$$\begin{cases} \frac{\partial G(\vec{r}|\vec{r}_{sce},\theta,\phi,t|t_{sce})}{\partial t} = -\vec{v}\cdot\vec{\nabla}G(\vec{r}|\vec{r}_{sce},\theta,\phi,t|t_{sce})) - MvG(\vec{r}|\vec{r}_{sce},\theta,\phi,t|t_{sce}) + \delta(\vec{r}-\vec{r}_{sce},\theta,\phi,t-t_{sce}) \\ \\ \frac{\partial w(\vec{r}_{sce},\theta,\phi,t)}{\partial t} = -\vec{v}\cdot\vec{\nabla}w(\vec{r}_{sce},\theta,\phi,t)) - Mvw(\vec{r}_{sce},\theta,\phi,t) + w_{sce}(\vec{r}_{sce},\theta,\phi,t) \\ \\ \forall\vec{r}_{sce}\in dV, \vec{r}_{sce}\in dV\, fixé \end{cases} \tag{4.1}$$

Les opérateurs agissent ici sur la coordonnée $\vec{r}_{sce}$

4.3 Exercice 3

Nous souhaitons maintenant nous intéresser au champ sonore existant au sein d'un local de forme non homogène. En l'occurrence, nous nous intéressons au cas d'un couloir, c'est à dire au cas d'une salle où l'une des dimensions est bien plus grande que les deux autres dimensions. Dans ces conditions, le champ sonore est supposé décroître le long de l'axe du couloir et être quasi-constant dans sa section.

Il est important de retenir les poins deux points suivants. (1) Le travail demandé doit reposer sur la condition aux limites donnée en équation 2.2. (2) Un travail similaire a été réalisé à partir de la condition aux limites 2.3 ; le lecteur peut retrouver ce travail au niveau des deux documents pdf donnés en annexe.

L'objectif ici consiste alors à établir un système d'équations simplifiées spécifiquement adapté à ce cas à partir des équations proposées.

Pour cela, la densité d'énergie acoustique pourrait être décomposée sur une base. Il pourrait s'agir d'une base de l'espace telle que :

$$w(\vec{r},\theta,\phi,t) = \sum_{p=0}^{\infty}\sum_{q=0}^{\infty}\sum_{s=0}^{\infty} f_{pqs}(\theta,\phi,t)P_p(x)P_q(y)P_s(z), \tag{4.2}$$

avec :

$$P_i(j) = \frac{1}{2^i i!}\frac{d^i}{dj^i}(j^2-1)^i, \tag{4.3}$$

$$f_{pqs}(\theta,\phi,t) = \int_{-\frac{L_z}{2}}^{\frac{L_z}{2}}\int_{-\frac{L_y}{2}}^{\frac{L_y}{2}}\int_{-\frac{L_x}{2}}^{\frac{L_x}{2}} f(\vec{r},\theta,\phi,t)P_p(x)P_q(y)P_s(z)dxdydz, \tag{4.4}$$

et la relation d'orthogonalité suivante :

$$\frac{1}{L_j}\int_{-\frac{L_j}{2}}^{\frac{L_j}{2}} P_m(j)P_n(j)dj = \sqrt{\frac{2}{2m+1}\frac{2}{2n+1}}\delta_{m,n}, \tag{4.5}$$

et le carré de la norme :

$$\|P_n(j)\|^2 = \frac{2}{2n+1}. \tag{4.6}$$

Une approche différente consisterait à décomposer la fonction de distribution sur une base orthonormale définies par les harmoniques sphériques normalisées $Y_{l,m}(\theta,\phi)$ (base sur les directions) :

$$w(\vec{r},\theta,\phi,t) = \sum_{l=0}^{+\infty}\sum_{m=-l}^{+l}\left(\frac{2l+1}{4\pi}\right)^{\frac{1}{2}} f_{l,m}(\vec{r},t)Y_{l,m}(\theta,\phi), \tag{4.7}$$

avec :

$$f_{l,m}(\vec{r},t) = \left(\frac{4\pi}{2l+1}\right)^{\frac{1}{2}}\int_0^{2\pi}\int_0^{\pi} w(\vec{r},\theta,\phi,t)Y^*_{l,m}(\theta,\phi)\sin\theta d\theta d\phi, \tag{4.8}$$

avec :

$$Y^*_{l,-m}(\theta,\phi) = (-1)^{-m}\times Y_{l,m}(\theta,\phi), \tag{4.9}$$

où $Y_{l,m}(\theta,\phi)$ sont des fonctions orthogonales définies à partir des Polynômes de Legendre $P_{l,m}$ de degré l et d'ordre m :

$$Y_{l,m}(\theta,\phi) = \left[\frac{2l+1}{4\pi}\frac{(l-m)!}{(l+m)!}\right]^{\frac{1}{2}} P_{l,m}(\cos\theta)e^{jm\phi}. \tag{4.10}$$

Ainsi, le champ sonore diffus, introduit précédemment, champ identique en tous points et en toutes directions, correspond finalement à l'ordre zéro de la base de l'espace (car $P_0(x) = P_0(y) = P_0(z) = 1$) ou de la base des directions (car $P_{0,0}(\cos\theta) = 1$).

La complexité du problème dans le choix judicieux de la base afin que les équations simplifiées obtenues soient physiquement représentatives du cas étudié (couloir).

4.4 Résultats connus pour un couloir

Nous donnons ici les résultats connus sur ce type de local afin d'aider à l'établissement des fonctions de base. Le couloir considéré est de longueur L_x et de section transversale $L_y \times L_z$.

4.4.1 Etude du niveau de la densité

La figure 4.1 montre (a) un couloir de dimensions [2 : 24 : 3], (j) un local plat de dimensions [12 : 18 : 3] et (m) une salle de dimensions homogènes [12 : 12 : 12].

La figure 4.2 montre l'influence du coefficient de diffusivité d sur le niveau de densité d'énergie $10\log(w(\vec{r}))$ pour le cas du régime permanent. La courbe « Diffusion »n'est pas à tenir compte. Ces courbes sont issues d'une approche de tir de rayons que nous considérons ici de référence. La source sonore est placée à 1 m d'une paroi (point rouge sur la figure 4.1).

La densité d'énergie $w(\vec{r})$ s'écrit ici :

$$w(\vec{r}) = \int_0^{2\pi}\int_0^{\pi} w(\vec{r},\vec{v})\sin\theta d\theta d\phi. \tag{4.11}$$

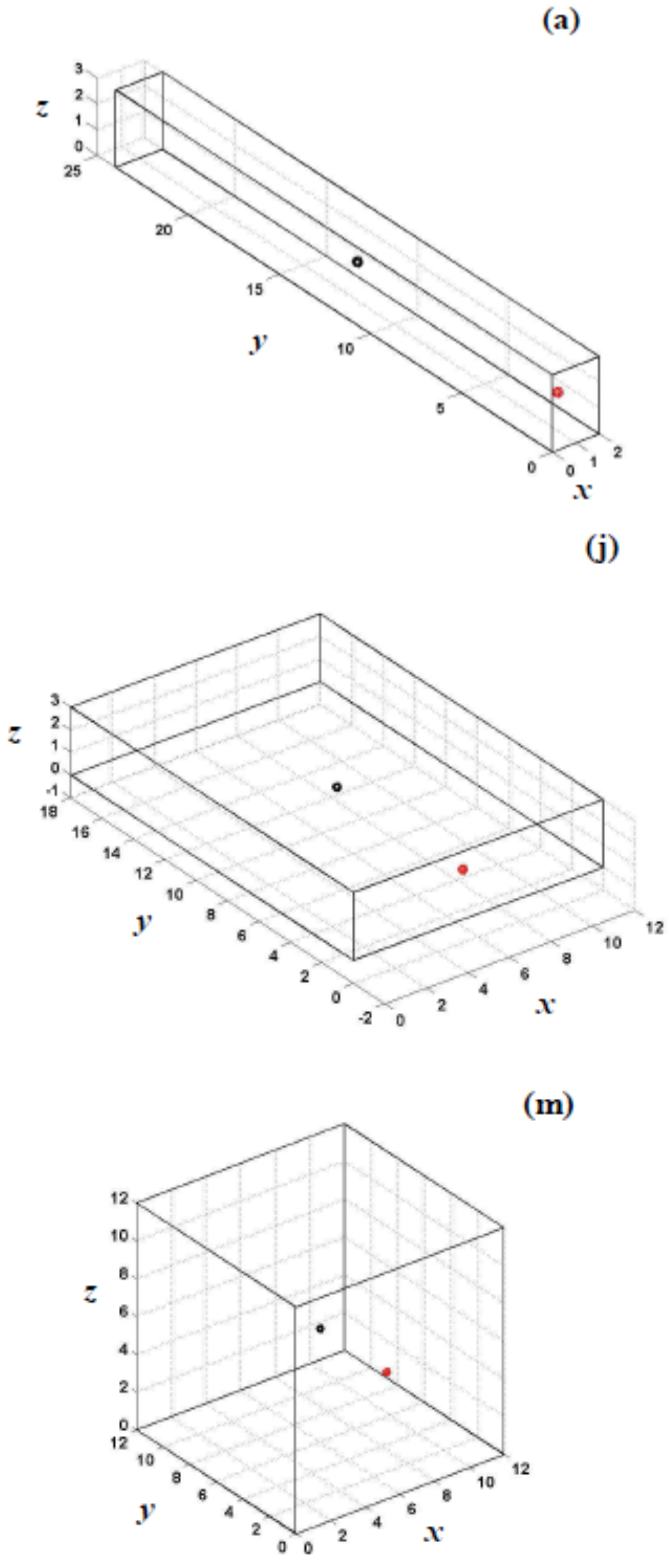

FIGURE 4.1 – (a) couloir [2 : 24 : 3] ; (j) local plat [12 : 18 : 3] ; (m) salle homogène [12 : 12 : 12].

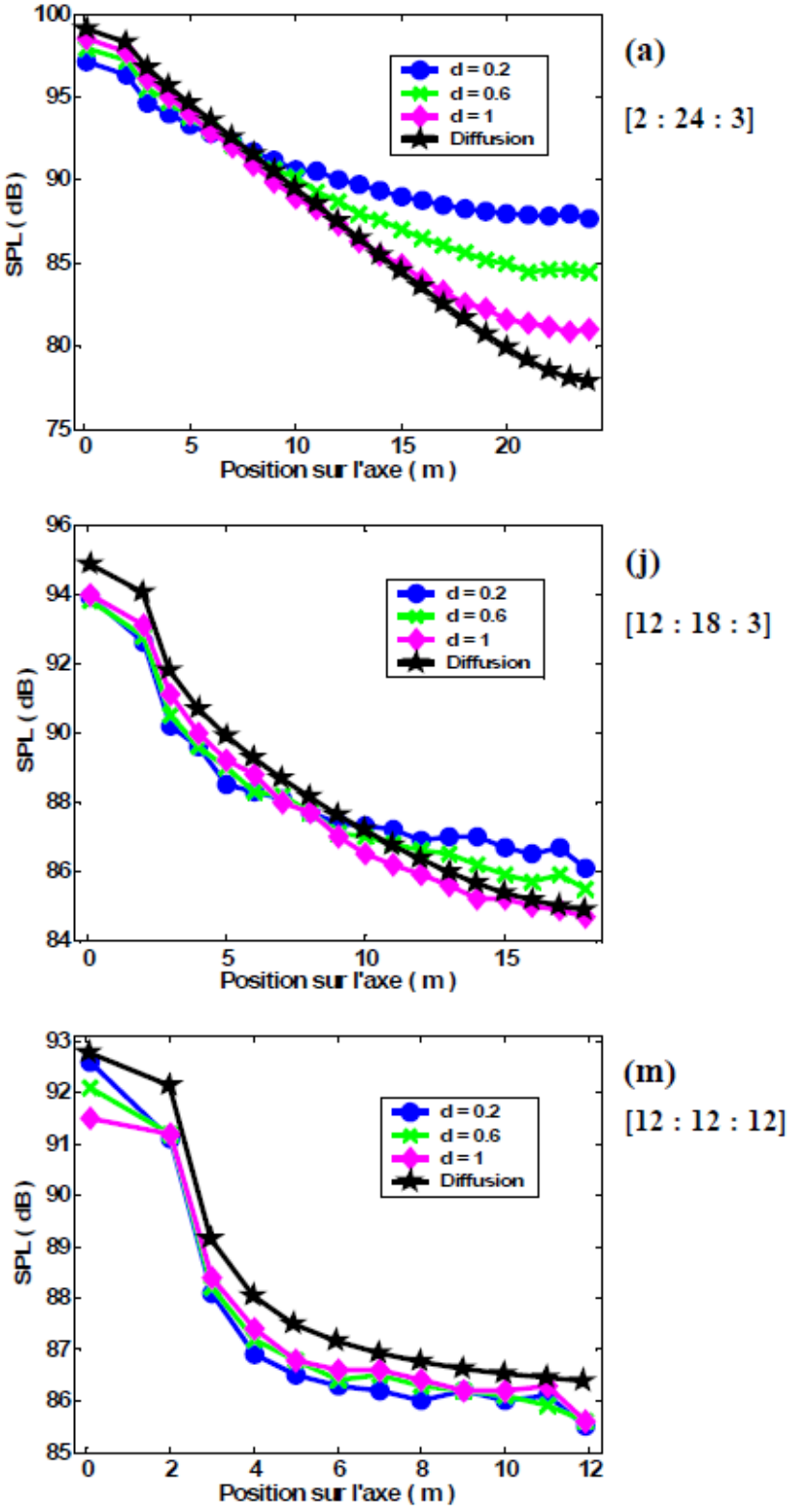

FIGURE 4.2 – Niveau de densité d'énergie $10\log(w(\vec{r}))$ lorsque le coefficient de diffusivité d est égal à 0.2, 0.6 et 1. La courbe « Diffusion »n'est pas à tenir compte.

4.4.2 Autres résultats

Le rapport :

$$\frac{D(\vec{r})}{\frac{4Vv}{3S}} = \frac{\left\|\vec{I}(\vec{r})\right\|}{\left\|\vec{\nabla}w(\vec{r})\right\|} \tag{4.12}$$

a été étudié et estimé pour le cas de couloirs avec une approche numérique de tir de particules (régime permanent). Nous donnons les résultats ci-dessous. Il faut noter que ces grandeurs sont celles moyennées sur tout les directions de propagation soit :

$$\vec{I}(\vec{r}) = \iint_{0\,0}^{2\pi\pi} \vec{I}(\vec{r},\vec{v})\sin\theta d\theta d\phi = \iint_{0\,0}^{2\pi\pi} \vec{v}w(\vec{r},\vec{v},t)\sin\theta d\theta d\phi, \tag{4.13}$$

$$\vec{\nabla}w(\vec{r}) = \iint_{0\,0}^{2\pi\pi} \vec{\nabla}w(\vec{r},\vec{v})\sin\theta d\theta d\phi. \tag{4.14}$$

La figure 4.3 montre l'influence de la distance source - récepteur sur ce rapport. Le couloir considéré est de dimensions $[40:4:4]$. Le coefficient d'absorption α est égale à 0.1 et le coefficient de diffusivité d est égal à 1. Il est observé que ce rapport est égal à 1 lorsque la distance source - récepteur est faible. Il augmente ensuite linéairement.

La figure 4.4 montre l'influence de la longueur L_x du local. Le couloir considéré est de dimensions $[L_x:4:4]$; Le coefficient d'absorption α est égale à 0.1 et le coefficient de diffusivité d est égal à 1. Les couloirs pour $L_x = 20m$, $L_x = 40m$ et $L_x = 60m$ sont considérés. Il est observé que le rapport $\frac{D(\vec{r})}{\frac{4Vv}{3S}}$ suit la même loi quelque soit la longueur du local. Ceci suggère que ce rapport ne varie pas en fonction de la longueur du local.

La figure 4.5 montre l'influence de l'absorption α du local. Le couloir considéré est de dimensions $[40:4:4]$. Le coefficient de diffusivité d est égal à 1. Le coefficient d'absorption α est égal à 0.1, 0.2 et 0.4. Nous observons que ce rapport dépend de l'absorption du local ; plus celle-ci augmente, plus le rapport augmente. Ce phénomène est d'autant plus marqué que la distance source - récepteur est importante.

La figure 4.6 montre l'influence de la section transversale $L_y \times L_z$ local. Le couloir considéré est de dimensions $[40:L_y:L_z]$. Le coefficient de diffusivité d est égal à 1 et le coefficient d'absorption*s* est égal à 0.1. Nous étudions les sections transversales $L_y \times L_z = 6 \times 6m^2$, $L_y \times L_z = 4 \times 4m^2$ et $L_y \times L_z = 2 \times 2m^2$. Nous observons que ce rapport dépend de la section transversale du local ; plus celle-ci augmente, plus le rapport augmente. Ce phénomène est d'autant plus marqué que la distance source - récepteur est importante.

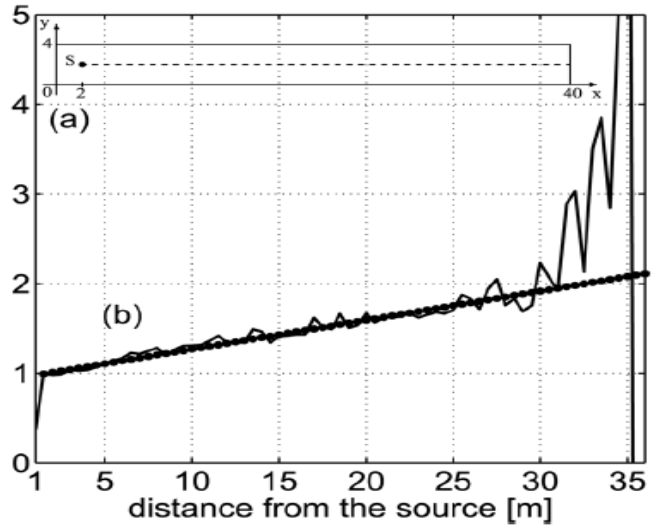

FIGURE 4.3 – Influence de la distance source / récepteur ; − : rapport estimé, • : approximation linéaire

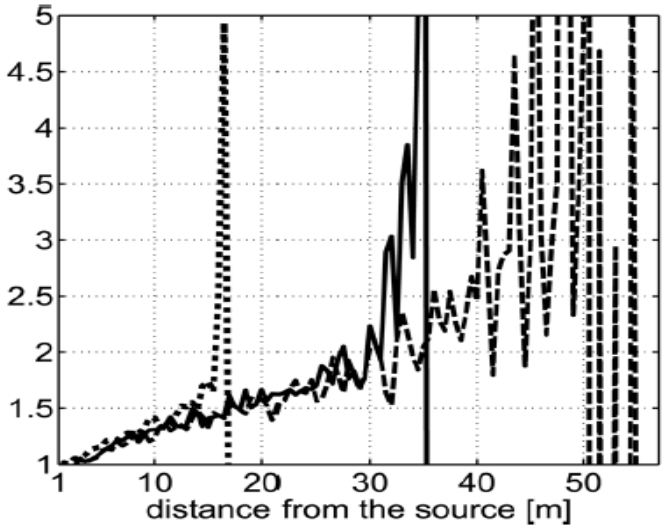

FIGURE 4.4 – Influence de la longueur L_x du local : le couloir considéré est de dimensions $[L_x : 4 : 4]$; la longueur est égale à (•) $L_x = 20m$, (−) $L_x = 40m$ et (−−) $L_x = 60m$.

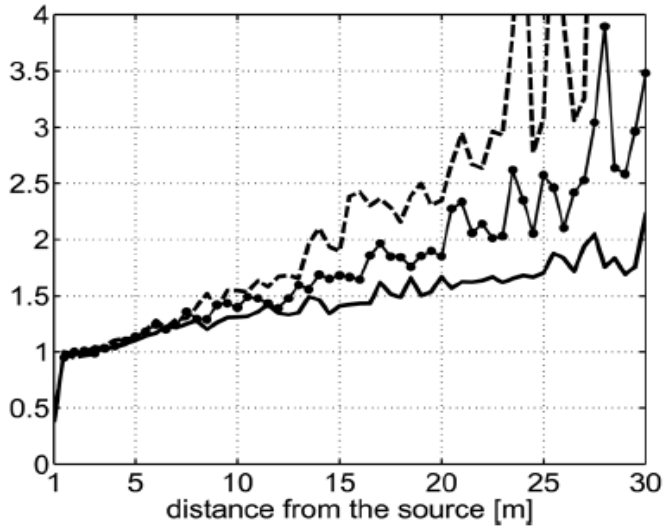

FIGURE 4.5 – Influence de l'absorption α du local. Le couloir considéré est dimensions $[40 : 4 : 4]$. Le coefficient de diffusivité d est égal à 1. Le coefficient d'absorption α est égal à $(-)$ 0.1, $(\bullet)$ 0.2 et $(--)$ 0.4.

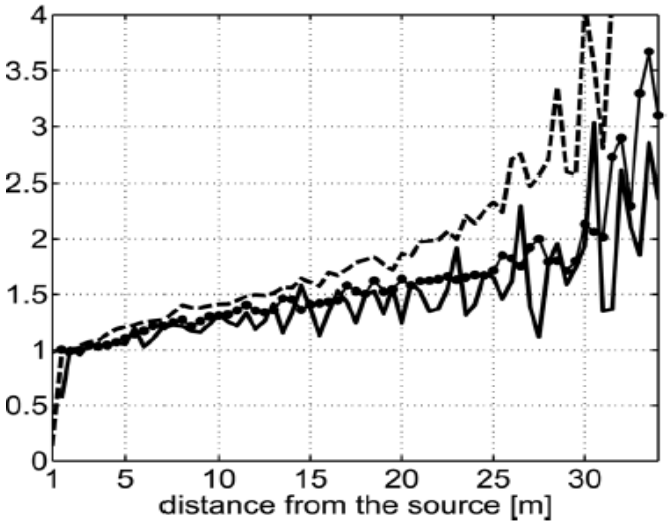

FIGURE 4.6 – Influence de la section transversale $L_y \times L_z$. Le couloir considéré est de dimensions $[40 : L_y : L_z]$. Le coefficient de diffusivité d est égal à 1 et le coefficient d'absorption est égal à 0.1. Nous étudions les sections transversales $(-)$ $L_y \times L_z = 6 \times 6$, $(\bullet)$ $L_y \times L_z = 4 \times 4$ et $(--)$ $L_y \times L_z = 2 \times 2$.

Annexe A

Articles de Jing

Cette annexe présente les travaux ayant été réalisés par Jing et al. à partir de la condition aux limites 2.3 et portant sur la décomposition du modèle sur une base adaptée au cas d'un couloir.

A.1 Article 1

One-dimensional transport equation models for sound energy propagation in long spaces: Theory

Yun Jing[a)]
Graduate Program of Architectural Acoustics, Rensselaer Polytechnic Institute, Troy, New York 12180

Edward W. Larsen
Department of Nuclear Engineering and Radiological Sciences, University of Michigan, Ann Arbor, Michigan 48109

Ning Xiang
Graduate Program of Architectural Acoustics, Rensselaer Polytechnic Institute, Troy, New York 12180

(Received 15 July 2009; revised 4 January 2010; accepted 5 January 2010)

In this paper, a three-dimensional transport equation model is developed to describe the sound energy propagation in a long space. Then this model is reduced to a one-dimensional model by approximating the solution using the method of weighted residuals. The one-dimensional transport equation model directly describes the sound energy propagation in the "long" dimension and deals with the sound energy in the "short" dimensions by prescribed functions. Also, the one-dimensional model consists of a coupled set of N transport equations. Only $N=1$ and $N=2$ are discussed in this paper. For larger N, although the accuracy could be improved, the calculation time is expected to significantly increase, which diminishes the advantage of the model in terms of its computational efficiency. © *2010 Acoustical Society of America.* [DOI: 10.1121/1.3298936]

PACS number(s): 43.55.Br, 43.55.Ka [EJS] Pages: 2312–2322

I. INTRODUCTION

Long spaces, in which one dimension is much larger than the other two, are of particular interest in room acoustics, as they usually take place in tunnels, underground stations, corridors, and some factories. Speech intelligibility and noise evaluation in these public places are critically important[1] and sometimes need to be predicted before construction.

The classical statistical theory, e.g., the Sabine equation, is not applicable in these situations because the sound field is highly nonuniform.[1,2] Other approaches, which fall into the category of the geometrical acoustic model, have recently been studied intensively, including the image source method,[3–5] the ray-tracing based method,[6,7] radiosity,[3,8,9] the diffusion equation model,[10–13] and the rendering equation model.[14] The image source method fails to include diffuse reflections, which have been found to be crucial when studying the steady-state and transient sound fields in long enclosures.[15] In contrast, the diffusion equation and original radiosity methods only take diffuse reflection into account. Although empirical modifications[16] have been applied to the diffusion equation method to model specular reflections, the model itself is inherently only suitable for low absorptive surfaces. The radiosity method can be modified to treat partially diffusely reflecting surfaces by combining the extended radiosity and mirror-image methods.[17] The ray-tracing based method is able to consider specular and diffuse reflections, but it is time-consuming due to its use of the Monte Carlo method. More recently Polles *et al.*[18,19] touched upon the transport theory in the context of urban streets. However, they did not formulate explicit solutions of the transport equations in their modeling effort rather than resort to asymptotic solutions in the form of diffusion equations.

The purpose of this work is to introduce a family of versatile one-dimensional transport equation models, which can simulate specular and diffuse reflections, air dissipations, scattering objects inside the enclosures, and different source types, as well as source directivities. These one-dimensional transport equations are (i) derived from a fundamental three-dimensional transport equation for sound propagation in enclosures and (ii) less computationally expensive than directly solving the three-dimensional transport equation since the number of independent spatial variables is reduced from 3 to 1.

All the theoretical considerations are presented in Sec. II. Although the mathematics is based on previous work in neutral particle transport,[20–22] differences are brought in by introducing several acoustic concepts. Specifically, different types of acoustic sources, boundary conditions at the two ends of a long space, and the specular reflections on side walls for a so-called two-group model are introduced for the first time in architectural acoustics.

This paper is structured as follows: first, Sec. II A presents the exact three-dimensional transport equation with corresponding boundary conditions. Then the method of weighted residuals is utilized to approximate the three-dimensional transport equation and simplify it to a coupled system of one-dimensional transport equations. Section II B discusses the details of the two simplest models, one having one one-dimensional transport equation, and the other having two coupled one-dimensional transport equations. The latter is shown through a simple test to be more accurate. Section

[a)]Author to whom correspondence should be addressed. Electronic mail: jingy@bwh.harvard.edu

 0001-4966/2010/127(4)/2312/11/$25.00

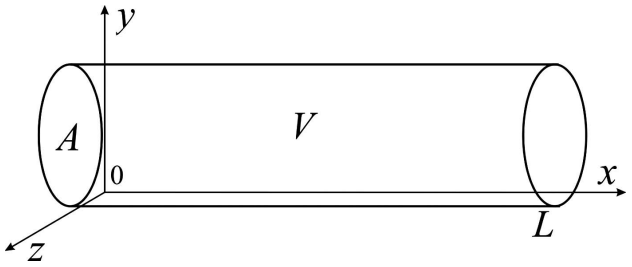

FIG. 1. Three-dimensional geometry of a long space.

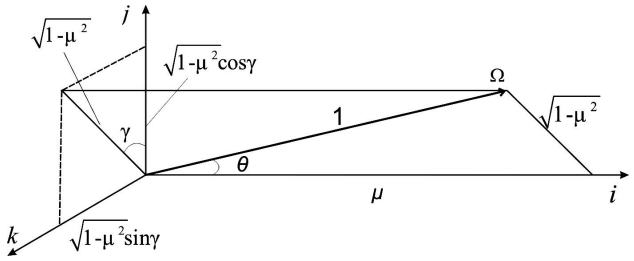

FIG. 2. Notations relevant to the transport equation.

II C also discusses the possibilities of modeling different sound sources and scattering objects inside the room. These would extend the application of the theory to a wider range of problems.

II. TRANSPORT EQUATION MODELS

In the geometrical acoustic model for room-acoustic predictions, the concept of sound waves is replaced by the notion of sound rays (or phonons[23]), which significantly reduces the difficulty of directly solving acoustic wave equations. The geometrical acoustic model is an energy-based method, which ignores complex wave phenomena including interference and diffraction. Sound is considered as rays propagating in straight lines with a certain amount of energy. This assumption is considered to be valid in the broad-band high frequency range, where the acoustic wavelength is much smaller than the room dimensions.

Under this circumstance, the sound energy can be described by the concept of a particle distribution function[19] $\psi(\boldsymbol{r},\boldsymbol{\Omega},t)$, where $\boldsymbol{r}$ is the position variable, $\boldsymbol{\Omega}$ is the angular variable, and t is time. More details of these variables are provided in Sec. II A. This particle distribution function can also be termed the sound energy angular flux, which is analogous to the term in neutral particle transport.

A. Three-dimensional transport equation model

This work considers a physical system consisting of a convex area A in the y,z-plane, extended in a "tubelike" or "ductlike" manner into the x-direction, creating a three-dimensional volume V (Fig. 1).

Assuming that V is "long and slender," implying that if the length L of the duct is finite, then

$$\frac{\sqrt{A}}{L} \ll 1. \tag{1}$$

Considering sound particle transport within the elongated volume V, in which the particle can be reflected specularly or diffusely (Lambert reflection) off the walls, the time-dependent transport equation is[19]

$$\frac{1}{c}\frac{\partial \psi}{\partial t}(\boldsymbol{r},\boldsymbol{\Omega},t) + \boldsymbol{\Omega}\cdot\boldsymbol{\nabla}\psi(\boldsymbol{r},\boldsymbol{\Omega},t) + M\psi(\boldsymbol{r},\boldsymbol{\Omega},t) = \frac{Q(\boldsymbol{r},t)}{4\pi},$$
$$0 < x < L \quad (y,z) \in A, \tag{2}$$

where ψ is the sound angular flux (W m^{-2} sr^{-1}), c is the speed of sound (m s^{-1}), Q is an isotropic sound source term (W m^{-3}), $\boldsymbol{\Omega}$ is the unit vector in direction of particle propagation, and M is the atmospheric attenuation constant (m^{-1}). The boundary condition for the long side walls is

$$\psi(\boldsymbol{r},\boldsymbol{\Omega},t) = R\left[(1-s)\psi(\boldsymbol{r},\hat{\boldsymbol{\Omega}},t) + \frac{s}{\pi}\int_{\boldsymbol{\Omega}'\cdot\boldsymbol{n}>0} \boldsymbol{\Omega}'\cdot\boldsymbol{n}\,\psi(\boldsymbol{r},\boldsymbol{\Omega}',t)d\Omega'\right],$$
$$0 < x < L \ , \ (y,z) \in \partial A, \ \boldsymbol{\Omega}\cdot\boldsymbol{n} < 0, \tag{3}$$

where R is the energy reflection coefficient ($R=1-\alpha$, where α is the absorption coefficient), s is the scattering coefficient, and $\boldsymbol{n}$ is the unit outer normal vector. The first term on the right side of Eq. (3) represents specular reflection, and the second (integral) term describes diffuse reflection. These terms are explained in more detail below. For simplicity in the following, all the walls have the same reflection and scattering coefficients. In addition, it is possible to include sound transmissions from adjacent rooms by adding an external source term.[24] However, this is beyond the scope of this work and will not be discussed further.

To explain the notation in these equations (Fig. 2), let $\boldsymbol{i}$, $\boldsymbol{j}$, and $\boldsymbol{k}$ denote the unit vector in the direction of the positive x-, y-, and z-axes, respectively, then the position variable (vector):

$$\boldsymbol{r} = (\vec{x},\vec{y},\vec{z}) = x\boldsymbol{i} + y\boldsymbol{j} + z\boldsymbol{k}. \tag{4}$$

Also, the unit vector in direction of flight

$$\boldsymbol{\Omega} = (\mu, \sqrt{1-\mu^2}\cos\,\gamma, \sqrt{1-\mu^2}\sin\,\gamma), \tag{5}$$

where

$$\mu = \cos\,\theta = \text{polar cosine}, \tag{6a}$$

$$\theta = \sphericalangle \text{ between } \boldsymbol{\Omega} \text{ and } \boldsymbol{i},$$

$$\gamma = \sphericalangle \text{ between the projection of } \boldsymbol{\Omega} \text{ onto the } \boldsymbol{j},\boldsymbol{k}\text{-plane and } \boldsymbol{j} = \text{azimuthal angle}. \tag{6b}$$

Equation (5) can be written as

$$\boldsymbol{\Omega} = \mu\,\boldsymbol{i} + \sqrt{1-\mu^2}\boldsymbol{\phi}, \tag{7}$$

where $\boldsymbol{\phi}$ is the unit vector

$$\boldsymbol{\phi} = \cos\,\gamma\boldsymbol{j} + \sin\,\gamma\boldsymbol{k}. \tag{8}$$

All the notations in Eq. (2) have now been defined.

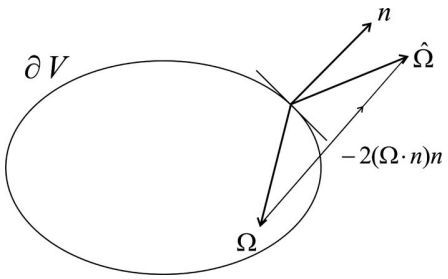

FIG. 3. Notations relevant to the specular reflection.

In Eq. (3), $\hat{\boldsymbol{\Omega}}$ is the "specular reflection" of the incident direction vector $\boldsymbol{\Omega}$ across the tangent plane at a point $\boldsymbol{r}$ on the boundary of V (Fig. 3), i.e.,

$$\hat{\boldsymbol{\Omega}} = \boldsymbol{\Omega} - 2(\boldsymbol{\Omega}\cdot\boldsymbol{n})\boldsymbol{n}. \tag{9}$$

Since $\boldsymbol{n}$ lies in the $\boldsymbol{j},\boldsymbol{k}$ plane, $\boldsymbol{n}\cdot\boldsymbol{i}=0$. Equation (9) yields

$$\hat{\mu} = \hat{\boldsymbol{\Omega}}\cdot\boldsymbol{i} = \boldsymbol{\Omega}\cdot\boldsymbol{i} = \mu, \tag{10}$$

and hence $\hat{\mu}=\mu$. When a particle specularly reflects, its μ-value does not change, but its γ-value does change. Equation (9) also implies that

$$\hat{\boldsymbol{\Omega}}\cdot\boldsymbol{n} = \boldsymbol{\Omega}\cdot\boldsymbol{n} - 2(\boldsymbol{\Omega}\cdot\boldsymbol{n}) = -\boldsymbol{\Omega}\cdot\boldsymbol{n}. \tag{11}$$

Thus, the projection of $\hat{\boldsymbol{\Omega}}$ onto $\boldsymbol{n}$ is positive, while the projection of $\boldsymbol{\Omega}$ onto $\boldsymbol{n}$ is negative and has the same magnitude.

In Eq. (3), $\boldsymbol{\Omega}'$ is a variable of integration that describes all the unit vectors in the outgoing directions. The integral term and the constant $1/\pi$ manifest that the reflected angular flux is uniform in all incoming directions (Lambert's law).[19] Furthermore, the constant s satisfies $0\le s\le 1$, and s represents the probability that when a particle scatters off the wall, it scatters diffusely, $(1-s)$ represents the probability that when a particle scatters off the wall, it scatters specularly.

Moreover, an operation on both sides of Eq. (3) by

$$\int_{\boldsymbol{\Omega}\cdot\boldsymbol{n}<0} |\boldsymbol{\Omega}\cdot\boldsymbol{n}|(\cdot)\,d\Omega \tag{12}$$

yields

$$\begin{aligned}\int_{\boldsymbol{\Omega}\cdot\boldsymbol{n}<0} |\boldsymbol{\Omega}\cdot\boldsymbol{n}|\psi(\boldsymbol{r},\boldsymbol{\Omega},t)\,d\Omega &= R\left[(1-s)\int_{\boldsymbol{\Omega}\cdot\boldsymbol{n}<0} |\boldsymbol{\Omega}\cdot\boldsymbol{n}|\psi(\boldsymbol{r},\hat{\boldsymbol{\Omega}},t)\,d\Omega\right.\\ &\left.+\frac{s}{\pi}\left(\int_{\boldsymbol{\Omega}\cdot\boldsymbol{n}<0} |\boldsymbol{\Omega}\cdot\boldsymbol{n}|\,d\Omega\right)\int_{\boldsymbol{\Omega}'\cdot\boldsymbol{n}>0} \boldsymbol{\Omega}'\cdot\boldsymbol{n}\,\psi\,d\Omega'\right].\end{aligned} \tag{13}$$

However,

$$\frac{1}{\pi}\int_{\boldsymbol{\Omega}\cdot\boldsymbol{n}<0} |\boldsymbol{\Omega}\cdot\boldsymbol{n}|\,d\Omega = \frac{1}{\pi}\int_0^{2\pi}\int_{-1}^{0} \mu\,d\mu\,d\gamma = 1. \tag{14}$$

Also, Eq. (11) and $d\hat{\Omega}=d\Omega$ yield

$$\int_{\boldsymbol{\Omega}\cdot\boldsymbol{n}<0} |\boldsymbol{\Omega}\cdot\boldsymbol{n}|\psi(\boldsymbol{r},\hat{\boldsymbol{\Omega}},t)\,d\Omega = \int_{\boldsymbol{\Omega}\cdot\boldsymbol{n}>0} \boldsymbol{\Omega}\cdot\boldsymbol{n}\,\psi(\boldsymbol{r},\boldsymbol{\Omega},t)\,d\Omega. \tag{15}$$

Thus, Eq. (13) becomes

$$\int_{\boldsymbol{\Omega}\cdot\boldsymbol{n}<0} |\boldsymbol{\Omega}\cdot\boldsymbol{n}|\psi(\boldsymbol{r},\boldsymbol{\Omega},t)\,d\Omega = R\int_{\boldsymbol{\Omega}\cdot\boldsymbol{n}>0} \boldsymbol{\Omega}\cdot\boldsymbol{n}\,\psi(\boldsymbol{r},\boldsymbol{\Omega},t)\,d\Omega, \tag{16}$$

implying that the rate per unit area, at which particles are reflected off the wall at $\mathbf{r}\in\partial V$, equals R times the rate per unit area, at which particles are incident on the wall at $\mathbf{r}\in\partial V$. Therefore, $0\le R\le 1$ and R represents the probability that when a particle strikes the wall it will be reflected (specularly or diffusely). This completes the interpretation of the terms in Eqs. (2) and (3).

Finally, for the boundary conditions of the two ends of the volume V, consider two models. The first model only takes specular reflections into account and is simply written as

$$\psi(0,y,z,\gamma,\mu,t) = R'\psi(0,y,z,\gamma,-\mu,t), \quad 0<\mu\le 1, \tag{17a}$$

$$\psi(L,y,z,\gamma,\mu,t) = R''\psi(L,y,z,\gamma,-\mu,t), \quad -1\le\mu<0, \tag{17b}$$

where R' and R'' are the reflection coefficients of the two ends, respectively.

For purely diffusely reflecting boundaries, according to Eq. (3),

$$\psi(\boldsymbol{r},\boldsymbol{\Omega},t) = \frac{R'(\text{or } R'')}{\pi}\int_{\boldsymbol{\Omega}'\cdot\boldsymbol{n}>0} \boldsymbol{\Omega}'\cdot\boldsymbol{n}\,\psi(\boldsymbol{r},\boldsymbol{\Omega}',t)\,d\boldsymbol{\Omega}', \quad \boldsymbol{\Omega}\cdot\boldsymbol{n}<0, \tag{18}$$

which leads to

$$\psi(0,y,z,\gamma,\mu,t) = \frac{R'}{\pi}\int_{\gamma'=0}^{2\pi}\int_{\mu'=-1}^{0} (-\mu')\psi(0,y,z,\gamma',\mu',t)\,d\mu'\,d\gamma', \quad 0<\mu\le 1, \tag{19a}$$

$$\psi(L,y,z,\gamma,\mu,t) = \frac{R''}{\pi}\int_{\gamma'=0}^{2\pi}\int_{\mu'=0}^{1} \mu'\psi(L,y,z,\gamma',\mu',t)\,d\mu'\,d\gamma', \quad -1\le\mu<0. \tag{19b}$$

For partially diffusely reflecting boundary condition, a linear combination of the above two is utilized.

B. One-dimensional transport approximation

To proceed, define

$$A' = \int\int_A dy\,dz = \text{cross-sectional area of } A,$$

$$L' = \int_{\partial A} ds' = \text{circumference of } A, \tag{20}$$

where ds' denotes an increment of arc length.

Combine Eqs. (2) and (7) to get

$$\frac{1}{c}\frac{\partial \psi}{\partial t}(\boldsymbol{r},\boldsymbol{\Omega},t) + \mu\frac{\partial \psi}{\partial x}(\boldsymbol{r},\boldsymbol{\Omega},t) + \sqrt{1-\mu^2}\boldsymbol{\phi}\cdot\nabla\psi(\boldsymbol{r},\boldsymbol{\Omega},t) + M\psi(\boldsymbol{r},\boldsymbol{\Omega},t) = \frac{Q(\boldsymbol{r},t)}{4\pi}. \tag{21}$$

Intuitively, a very simple way to arrive at a one-dimensional transport equation is to disregard the y, z-dependency of the distribution function ψ by setting the third term in Eq. (21) to zero. However, this would not give a correct one-dimensional transport equation. As shown below, keeping the third term in Eq. (21) is imperative when integrating Eq. (21) and the boundary condition, i.e., Eq. (3).

An approximation of ψ by the method of weighted residuals is then introduced as

$$\psi(\boldsymbol{r},\mu,\gamma,t) \approx \sum_{j=1}^{N} \alpha_j(y,z,\gamma)\psi_j(x,\mu,t), \tag{22}$$

where α_j are specified basis functions and ψ_j are unknown expansion functions. The criterion for selecting the basis functions is that: In a long space, it is reasonable to assume that the sound field is strongly dependent on the long dimension (x-axis) and weakly dependent on the lateral coordinates (y- and z-axes). In other words, it is expected that the sound field varies significantly along the long dimension but insignificantly across the cross section. Similarly, it is assumed that the angle dependence of sound angular flux on μ is much stronger than on γ. Therefore, it is decided to separate y, z, and γ from x and μ by using the basis functions, which are predefined. In this way, the original equation discards the y, z, and γ dependences and is only x and μ dependent.

Substituting the approximation of ψ generates an error or a residual, which is required to be orthogonal to certain weight functions, $\beta_i(y,z,\gamma)$ $(1 \le i \le N)$. Equivalently, the method of weighted residuals forces the residual to zero in an average way over a certain domain, which leads to minimum error.

To explicitly show this and determine the equations for the ψ_j, an operation on both sides of Eq. (21) by $\int\int_A \int_{\gamma=0}^{2\pi} \beta_j(\cdot)d\gamma dydz$ and an operation on both sides of Eq. (3) by $\int_{\partial A}\int_{\boldsymbol{\phi}\cdot\boldsymbol{n}<0}\beta_j(\cdot)d\gamma ds$ yield

$$\int\int_A \int_{\gamma=0}^{2\pi} \beta_j\left[\frac{1}{c}\frac{\partial\psi}{\partial t} + \mu\frac{\partial\psi}{\partial x} + \sqrt{1-\mu^2}\boldsymbol{\phi}\cdot\nabla\psi + M\psi - \frac{Q(\boldsymbol{r},t)}{4\pi}\right]d\gamma dydz = 0, \tag{23}$$

$$\int_{\partial A}\int_{\boldsymbol{\phi}\cdot\boldsymbol{n}<0}\beta_j\left\{\psi - R\left[(1-s)\psi + \frac{s}{\pi}\int_{\boldsymbol{\Omega}'\cdot\boldsymbol{n}>0}\boldsymbol{\Omega}'\cdot\boldsymbol{n}\psi d\Omega'\right]\right\}d\gamma ds' = 0. \tag{24}$$

In addition, α_j and β_i are assumed to satisfy

$$\frac{1}{2\pi A'}\int_A\int_0^{2\pi}\alpha_j\beta_i d\gamma dydz = \delta_{ij}, \quad 1 \le i, \quad j \le N, \tag{25}$$

where δ_{ij} is the Kronecker delta. Equations (22) and (25) imply that

$$\psi_i = \frac{1}{2\pi A'}\int_A\int_0^{2\pi}\beta_i\psi d\gamma dydz, \quad 1 \le i \le N. \tag{26}$$

For a point source at $\boldsymbol{r}_0=(x_0,y_0,z_0)$, i.e., $Q(\boldsymbol{r},t) = Q(t)\delta(x-x_0)\delta(y-y_0)\delta(z-z_0)$, apply the divergence theorem to Eq. (23), then use Eq. (24), and finally arrive at the following set of N transport equations (see Appendix for details):

$$\frac{1}{c}\frac{\partial\psi_i}{\partial t} + \mu\frac{\partial\psi_i}{\partial x} + M\psi_i + \sqrt{1-\mu^2}\sum_{j=1}^{N}a_{ij}\psi_j = \frac{2Rs}{\pi}\sqrt{1-\mu^2}\sum_{j=1}^{N}b_{ij}\int_{-1}^{1}\sqrt{1-\mu'^2}\psi_j(\mu')d\mu' + Q_i, \tag{27}$$

where the derivation of a_{ij} and b_{ij} can be found in the Appendix. For example,

$$a_{ij} = \frac{1-R(1-s)}{2\pi A'}\left[\int_{\partial A}\int_{\boldsymbol{\phi}\cdot\boldsymbol{n}>0}\boldsymbol{\phi}\cdot\boldsymbol{n}\beta_i\alpha_j d\gamma ds'\right], \quad i = 1 \tag{28}$$

$$b_{ij} = \frac{1}{4\pi A'}\int_{\partial A}\left(\int_{\boldsymbol{\phi}\cdot\boldsymbol{n}<0}|\boldsymbol{\phi}\cdot\boldsymbol{n}|\beta_i d\gamma\right)\times\left(\int_{\boldsymbol{\phi}\cdot\boldsymbol{n}>0}\boldsymbol{\phi}\cdot\boldsymbol{n}\alpha_j d\gamma\right)ds' \quad \text{for } 1 \le i \le 2, \tag{29}$$

and

$$Q_i = \frac{1}{2\pi A'}\int_A\int_0^{2\pi}\beta_i\frac{Q(t)\delta(\boldsymbol{r}-\boldsymbol{r}_0)}{4\pi}d\gamma dydz. \tag{30}$$

In addition, substitution of Eqs. (17a) and (17b) into Eq. (26) yields the purely specular boundary condition for the two ends as

$$\psi_i(0,\mu,t) = R'\psi_i(0,-\mu,t), \quad 0 < \mu \le 1, \tag{31a}$$

$$\psi_i(L,\mu,t) = R''\psi_i(L,-\mu,t), \quad -1 \le \mu < 0. \tag{31b}$$

Similarly, for diffuse reflection,

$$\psi_i(0,\mu,t) = \frac{R'}{\pi}\times\frac{1}{2\pi A'}\int_A\int_0^{2\pi}\beta_i\left[\int_0^{2\pi}\int_{-1}^{0}(-\mu')\times\psi(0,y,z,\mu',\gamma',t)d\mu' d\gamma'\right]d\gamma dydz, \quad 0 < \mu \le 1, \tag{32a}$$

$$\psi_i(L,\mu,t) = \frac{R''}{\pi} \times \frac{1}{2\pi A'} \int_A \int_0^{2\pi} \beta_i \left[\int_0^{2\pi} \int_0^1 \mu' \psi(0,y,z, \mu',\gamma',t) d\mu' d\gamma' \right] d\gamma dy dz, \quad -1 \le \mu < 0, \tag{32b}$$

Now the exact three-dimensional equations, i.e., Eqs. (2) and (3), have been reduced to a coupled set of N one-dimensional transport equations, in the expectation that the resulting computation will be less cumbersome. In this set of equations, α_j and β_i have to be specified. Large N should increase the computational load but should also reduce the error of the approximation. Thus, the choice of N, the number of transport equations in the approximate one-dimensional model, is a compromise between computational effort and accuracy. This study only considers $N=1$ and 2, which are treated in detail below.

1. One-group model ($N=1$)

This subsection begins with the choice of the basis functions and weight functions. There are different ways to select these functions, for example, the collocation method (the weight functions are chosen to be Dirac delta functions), the least-squares method (which uses derivatives of the residual itself as weight functions), and the Galerkin method.[25] The Galerkin method is preferred because it has already been shown to be accurate for this specific transport equation model.[22] In the Galerkin method, the weight functions are chosen to be identical to the basis functions, and for $N=1$

$$\alpha_1(y,z,\gamma,t) = \beta_1(y,z,\gamma,t) = 1. \tag{33}$$

The constant of 1 is a convenient choice suggested in previous work.[22] Thus

$$\psi(\boldsymbol{r},\mu,\gamma,t) \approx \psi_1(x,\mu,t). \tag{34}$$

Based on this equation, the three-dimensional transport equation is reduced to a truly "one-dimensional model" since the y and z coordinates disappear. It indicates that the y, z, and γ-dependences of ψ are weak; i.e., the energy is almost uniform in the y-z plane and over the γ angle. This is expected to be a good approximation when the absorption on the boundary is weak and the long space is sufficiently narrow. The theoretical demonstration of this statement has been given in Ref. 22, which is conveyed in a rather mathematical way. It might be more illustrating to explain this from the acoustic point of view: if the absorption on the side walls are strong, the variation in the sound energy across the cross section will be significant, which has been shown in previous literatures, e.g., Ref. 12. This implies that the sound energy is no more weakly y- and z-dependent, which violates the assumption of the one-group model. It has also been theoretically proved that this approximation is valid if the receiver is sufficiently far away from the ends of the long space.[22] Substitution of Eq. (33) into Eqs. (28) and (29) yields

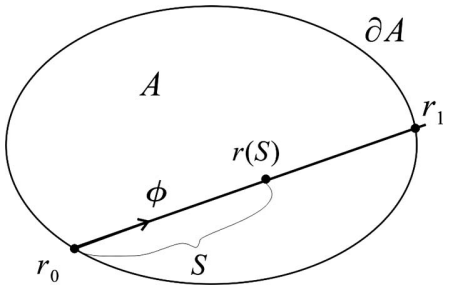

FIG. 4. Notations relevant to function D.

$$a_{11} = [1 - R(1-s)]\frac{L'}{\pi A'}, \quad b_{11} = \frac{L'}{\pi A'}. \tag{35}$$

The one-dimensional transport equation model for $N=1$ is then

$$\frac{1}{c}\frac{\partial \psi_1}{\partial t} + \mu \frac{\partial \psi_1}{\partial x} + \left[M + \sqrt{1-\mu^2}\frac{1-R(1-s)}{\lambda} \right] \psi_1 = \frac{2Rs}{\lambda \pi}\sqrt{1-\mu^2} \int_{-1}^{1} \sqrt{1-\mu'^2}\psi_1(\mu')d\mu', \tag{36}$$

where

$$\lambda = \frac{\pi A'}{L'}. \tag{37}$$

The specular boundary conditions for the two ends are

$$\psi_1(0,\mu,t) = R'\psi_1(0,-\mu,t), \quad 0 < \mu \le 1, \tag{38a}$$

$$\psi_1(L,\mu,t) = R''\psi_1(L,-\mu,t), \quad -1 \le \mu < 0. \tag{38b}$$

Also, the diffuse boundary conditions are

$$\psi_1(0,\mu,t) = 2R' \int_{-1}^{0} (-\mu')\psi_1(0,\mu',t)d\mu', \quad 0 < \mu \le 1, \tag{39a}$$

$$\psi_1(L,\mu,t) = 2R'' \int_0^1 \mu' \psi_1(L,\mu',t)d\mu', \quad -1 \le \mu < 0. \tag{39b}$$

This one-group one-dimensional transport equation is the same for two different structures having the same ratio of A' to L'.

To explain the physical interpretation of the constant λ in Eq. (37), a function $D(y,z,\boldsymbol{\phi})$ is defined as the distance from a point (x,y,z) in the interior of the volume to the inner wall in the direction $-\boldsymbol{\phi}$ so that

$$\boldsymbol{\phi} \cdot \nabla D(y,z,\boldsymbol{\phi}) = 1 \quad (y,z) \in A, \tag{40a}$$

$$D(y,z,\boldsymbol{\phi}) = 0 \quad (y,z) \in \partial A, \quad \boldsymbol{\phi} \cdot \boldsymbol{n} < 0, \tag{40b}$$

where $\boldsymbol{n}$ is the unit outer normal vector. If $\boldsymbol{r}_0 = (x,y,z) \in \partial A$ and $\boldsymbol{\phi} \cdot \boldsymbol{n} < 0$ (i.e., $\boldsymbol{\phi}$ points into A), then on the line $\boldsymbol{r}(S) = \boldsymbol{r}_0 + S\boldsymbol{\Omega}$, Eq. (40) yields $D[\boldsymbol{r}(S),\boldsymbol{\phi}] = S$ (Fig. 4).

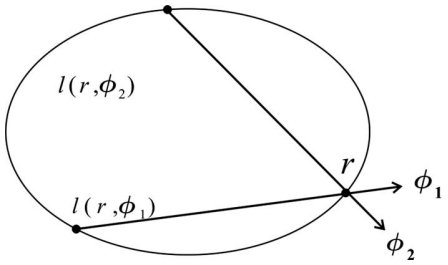

FIG. 5. Notations relevant to function l.

At the point $\boldsymbol{r}_1 \in \partial A$, where the line "exits" A, $D(\boldsymbol{r}_1,\boldsymbol{\phi})=|\boldsymbol{r}_1-\boldsymbol{r}_0|=$distance through A in the direction $\boldsymbol{\phi} \equiv l(\boldsymbol{r}_1,\boldsymbol{\phi})$ (Fig. 5).

Now an operation on both sides of Eq. (40a) by $\int_A \int_{\gamma=0}^{2\pi}(\cdot)d\gamma dydz$ yields

$$\begin{aligned} 2\pi A &= \int_A \int_{\gamma=0}^{2\pi} \boldsymbol{\phi}\cdot\nabla D d\gamma dxdy \\ &= \int_{\gamma=0}^{2\pi}\left(\int_{\partial A} \boldsymbol{n}\cdot\boldsymbol{\phi} D ds'\right)d\gamma \\ &= \int_{\partial A}\left(\int_{\boldsymbol{\phi}\cdot\boldsymbol{n}>0} \boldsymbol{n}\cdot\boldsymbol{\phi} D d\gamma\right)ds' \\ &= \int_{\partial A}\int_{\boldsymbol{\phi}\cdot\boldsymbol{n}>0} \boldsymbol{n}\cdot\boldsymbol{\phi} l(\boldsymbol{r},\boldsymbol{\phi}) d\gamma ds'. \end{aligned} \tag{41}$$

But also,

$$\int_{\partial A}\left(\int_{\boldsymbol{\phi}\cdot\boldsymbol{n}>0} \boldsymbol{\phi}\cdot\boldsymbol{n} d\gamma\right)ds' = \int_{\partial A} 2ds' = 2L'. \tag{42}$$

Hence, λ has the geometrical interpretation:

$$\lambda = \langle l\rangle = \frac{\int_{\partial A}\int_{\boldsymbol{\phi}\cdot\boldsymbol{n}>0} \boldsymbol{n}\cdot\boldsymbol{\phi} l(\boldsymbol{r},\boldsymbol{\phi}) d\gamma ds'}{\int_{\partial A}\int_{\boldsymbol{\phi}\cdot\boldsymbol{n}>0} \boldsymbol{n}\cdot\boldsymbol{\phi} d\gamma ds'} = \frac{\pi A'}{L'}, \tag{43}$$

which is the classical diffuse mean free path length for two dimensions,[26] or mean chord length[27] across A. This completes the discussion of the one-group transport equation model.

2. Two-group model ($N=2$)

The choice of the basis functions and weight functions for the two-group model ($N=2$) is based on a linear combination of the constant function 1, and $D(y,z,\gamma)$, defined in Sec. II B 1 to be the distance from a point (x,y,z) in the interior of the volume to the inner wall in the direction $-\boldsymbol{\phi}$. They are expressed explicitly as

$$\alpha_1(y,z,\gamma,t) = \beta_1(y,z,\gamma,t) = 1, \tag{44}$$

$$\alpha_2(y,z,\gamma,t) = \beta_2(y,z,\gamma,t) = u[D(y,z,\boldsymbol{\phi}) - v], \tag{45}$$

where

$$u = \left\{\frac{1}{2\pi A'}\int_A\int_0^{2\pi}[D(y,z,\boldsymbol{\phi})-v]^2 d\gamma dydz\right\}^{-1/2}, \tag{46}$$

$$v = \frac{1}{2\pi A'}\int_A\int_0^{2\pi} D(y,z,\boldsymbol{\phi}) d\gamma dydz, \tag{47}$$

or in the form of curve integral:

$$u = \left[\frac{1}{6\pi A'}\int_{\partial A}\int_0^{2\pi} \boldsymbol{\phi}\cdot\boldsymbol{n}(D-v)^3 d\gamma ds'\right]^{-1/2}, \tag{48}$$

$$v = \frac{1}{4\pi A'}\int_{\partial A}\int_{\boldsymbol{\phi}\cdot\boldsymbol{n}>0} \boldsymbol{\phi}\cdot\boldsymbol{n} D^2 d\gamma ds', \tag{49}$$

which can be obtained using the divergence theorem (Gauss's theorem) and the identity[22]

$$D = (\boldsymbol{\phi}\cdot\nabla D^2)/2. \tag{50}$$

To show how to derive the matrices a_{ij} and b_{ij}, using a_{12} as an example:

$$\begin{aligned} a_{12} &= \frac{1-R(1-s)}{2\pi A'}\int_{\partial A}\int_{\boldsymbol{\phi}\cdot\boldsymbol{n}>0} \boldsymbol{\phi}\cdot\boldsymbol{n} u(D-v) d\gamma ds' \\ &= \frac{1-R(1-s)}{2\pi A'} u\left(\int_{\partial A}\int_0^{2\pi} \boldsymbol{\phi}\cdot\boldsymbol{n} D d\gamma ds' \right. \\ &\quad \left. - \int_{\partial A}\int_{\boldsymbol{\phi}\cdot\boldsymbol{n}>0} \boldsymbol{\phi}\cdot\boldsymbol{n} d\gamma ds'\right) \\ &= \frac{1-R(1-s)}{2\pi A'} u\left(\int_A\int_0^{2\pi} \boldsymbol{\phi}\cdot\nabla D d\gamma dydz - v2L'\right) \\ &= [1-R(1-s)]\left(u - uv\frac{L'}{\pi A'}\right). \end{aligned} \tag{51}$$

In similar fashion, other matrix elements can be derived. Omitting the lengthy algebra, the final results of the matrices a_{ij} and b_{ij} can be expressed as

$$\begin{aligned} a_{11} &= [1-R(1-s)]\frac{L'}{\pi A'}, \\ a_{12} &= [1-R(1-s)]\left(u - uv\frac{L'}{\pi A'}\right), \\ a_{21} &= [R(1-s)-1]\frac{uvL'}{\pi A'}, \\ a_{22} &= \frac{u^2v^2L'}{\pi A'} + R(1-s)uv\left(u - \frac{uvL'}{\pi A'}\right), \end{aligned} \tag{52}$$

$$b_{ij} = \begin{bmatrix} L'/(\pi A') & u - uvL'/(\pi A') \\ -uvL'/(\pi A') & -uv[u - uvL'/(\pi A')] \end{bmatrix}. \tag{53}$$

The specular boundary conditions on the two ends are

$$\psi_1(0,\mu,t) = R'\psi_1(0,-\mu,t), \quad 0<\mu\le 1, \tag{54a}$$

$$\psi_1(L,\mu,t) = R''\psi_1(L,-\mu,t), \quad -1 \le \mu < 0, \tag{54b}$$

$$\psi_2(0,\mu,t) = R'\psi_2(0,-\mu,t), \quad 0 < \mu \le 1, \tag{54c}$$

$$\psi_2(L,\mu,t) = R''\psi_2(L,-\mu,t), \quad -1 \le \mu < 0. \tag{54d}$$

The diffuse boundary conditions are given by

$$\psi_1(0,\mu,t) = 2R'\int_{-1}^{0}(-\mu')\psi_1(0,\mu',t)d\mu', \quad 0 < \mu \le 1, \tag{55a}$$

$$\psi_1(L,\mu,t) = 2R''\int_{0}^{1}\mu'\psi_1(0,\mu',t)d\mu', \quad -1 \le \mu < 0, \tag{55b}$$

$$\psi_2(0,\mu,t) = \frac{R'u^2}{2\pi^2A'}\left[\int_A\left(\int_0^{2\pi}Dd\gamma\right)^2 dydz - 4\pi^2v^2A'\right] \times \int_{-1}^{0}-\mu'\psi_2(0,\mu',t)d\mu', \quad 0 < \mu \le 1, \tag{55c}$$

$$\psi_2(L,\mu,t) = \frac{R''u^2}{2\pi^2A'}\left[\int_A\left(\int_0^{2\pi}Dd\gamma\right)^2 dydz - 4\pi^2v^2A'\right] \times \int_{0}^{1}\mu'\psi_2(0,\mu',t)d\mu', \quad -1 \le \mu < 0, \tag{55d}$$

where for a long space with circular cross section A, u, and v are given analytically as

$$u = 3\pi(9\pi^2 - 64)^{-1/2}/\rho' \quad \text{and} \quad v = 8\rho'/(3\pi), \tag{56}$$

with ρ' being the radius of the circle. a_{ij} and b_{ij} are then immediately known by employing Eqs. (52) and (53). For noncircular geometries, u and v can either be analytically or numerically derived. For instance, implementing Eqs. (48) and (49) for a square of width of d yields

$$u \approx 3.25/d \quad \text{and} \quad v \approx 0.47d. \tag{57}$$

Comparing the one-group and two-group models, the latter has an additional transport equation, which increases its complexity. However, the accuracy should also be increased, since the energy is not assumed to be uniform in the y-z plane or over the γ angle as the one-group model does. While the one-group model is legitimate when absorption is weak, the two-group model should be valid for a wider range of absorption coefficients. In addition, the function D distinguishes different types of cross-sectional geometry by generating different u and v, and it brings back the coordinates y, z, and γ. Thus the two-group model allows the consideration of the positions of both a receiver and source in the y-z plane.

Next, consider a simple numerical example to compare the accuracy of the one-group and two-group models. Assuming a semi-infinite circular duct with a radius of 1 m, and having all the surfaces perfectly absorbing, the sound energy decay along the long dimension is investigated when an omnidirectional point source is located at the center of the origin ($x=y=z=0$). This problem is equivalent to the sound propagation from a point source to a free space, where the sound field can be analytically solved. Therefore, we can use the exact analytic solution as the benchmark.

By assigning the reflection coefficient R and the attenuation coefficient M to zero in the one-group model, the analytic solution can be obtained as

$$\psi_1(x,\mu) = \frac{Q}{4\pi A'\mu}\exp\left(-x\frac{\sqrt{1-\mu^2}}{\lambda\mu}\right), \tag{58}$$

where Q is the sound source power, and the time t is discarded since the steady-state solution is of concern in this case. For the two-group model, a numerical solution is obtained. A follow-up paper[28] will report on details of the numerical implementations.

So far only the angular flux ψ has been discussed. However, in room acoustics, the sound energy or the sound pressure level is most frequently focused. Knowing the angular flux ψ, the sound pressure level can be written as[29]

$$L_p(\boldsymbol{r}) = 10\log\left[\frac{I(\boldsymbol{r})\rho c}{P_{\text{ref}}^2}\right], \tag{59}$$

where

$$I = \int_0^{2\pi}\int_{-1}^{1}\psi d\mu d\gamma \tag{60}$$

is the magnitude of sound intensity, ρ is the air density, and $P_{\text{ref}}=2\times10^{-5}$ Pa is the pressure reference. Thus, the intensity is an integral of the angular flux over all the angles. While the Monte Carlo simulation normally only provides the sound energy, which is angularly independent, the transport equation model provides more detailed angular information through the angular flux ψ.

By numerically implementing Eq. (60) for the solutions of the one-group and two-group models, the sound intensities along the long dimension can be obtained and are plotted in Fig. 6. These solutions are normalized at a distance of 1 m to the source. The exact solution $\psi(\boldsymbol{r},\boldsymbol{\Omega})$ of Eq. (2) with $\partial\psi/\partial t=0$, $M=0$, and $Q(\boldsymbol{r})=Q\delta(\boldsymbol{r})$ satisfies

$$\int_0^{2\pi}\int_{-1}^{1}\psi(\boldsymbol{r},\boldsymbol{\Omega})d\mu d\gamma = \frac{Q}{4\pi r^2}, \tag{61}$$

where $r=\sqrt{x^2+y^2+z^2}$ is the distance from the source. Figure 6 illustrates this result, which is normalized at $x=1$, as a benchmark. Figure 6(a) indicates that the two-group solution decays at a faster and more accurate rate than the one-group solution. It seems plausible that the one-group model is not such a bad match to the analytic solution at a long distance. However, Fig. 6(b), illustrating the sound intensity on a logarithmic scale, indicates that the one-group model becomes even worse at a long distance. Therefore, the one-group model is not able to accurately predict the sound field in this open-space case. This is because, as demonstrated in Sec. II B 1, the one-group model will fail when the absorption on

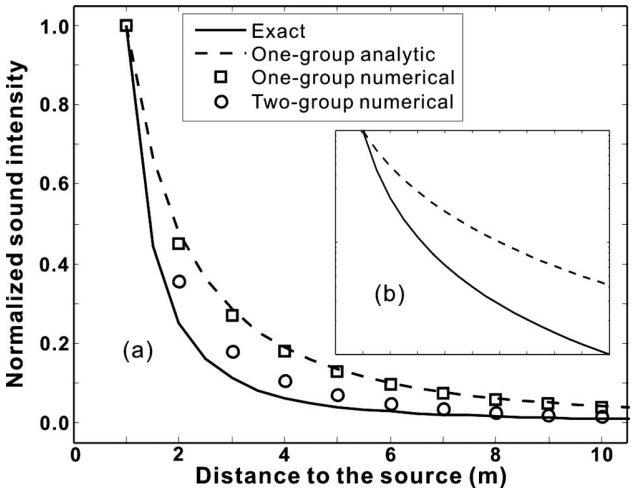

FIG. 6. Comparison of the sound intensity decay along the long dimension of a circular duct between the one-group model and the two-group model in a free space scenario. The analytic solution ($1/r^2$ law) is used as a benchmark. (a) The sound intensity is plotted on a linear scale. (b) The sound intensity is plotted on a logarithmic scale: only the exact solution and the analytic one-group model solution are presented.

the wall is strong (as in this case, where the absorption coefficient is 1.0). Additional simulations show that the numerical results of both one- and two-group models converge to the analytic solution when narrowing the duct.

Indeed, the sound propagation in a free space is somehow an unrealistic case. It is expected that the result would be totally different if the tube wall had been given a reflection coefficient close to 1, especially for the one-group model which is validated when the reflection is strong. However, the purpose of this example is only to demonstrate that the two-group model is more accurate than the one-group model. And the reason for choosing this simple example is that the analytic solutions of the one-group model as well as the three-dimensional exact equation can be easily found. More complicated cases (reflection coefficient being nonzero) require sophisticated numerical methods for both one- and two-group models, which will be detailed in a follow-up paper.[28]

C. Other considerations

1. Sources

This subsection briefly discusses the possibility of taking into account different types of sound sources and source directivity. This demonstrates the flexibility of the present model.

So far, only the omnidirectional point source has been considered. According to Eq. (30) and the definition of the Dirac delta function, for the two-group model,

$$Q_1 = \frac{Q(t)}{4\pi A'}\delta(x-x_0), \tag{62a}$$

$$Q_2 = \frac{Q(t)}{8\pi^2 A'}\delta(x-x_0)\times\int_0^{2\pi} u[D(y_0,z_0,\boldsymbol{\phi})-v]d\gamma. \tag{62b}$$

For a point source at $\boldsymbol{r}_0$ with directivity, the source term in Eq. (2) is written as $Q(\gamma,\mu,t)\delta(\boldsymbol{r}-\boldsymbol{r}_0)$ instead, and similarly

$$Q_1 = \frac{1}{2\pi A'}\delta(x-x_0)\int_0^{2\pi} Q(\gamma,\mu,t)d\gamma, \tag{63a}$$

$$Q_2 = \frac{1}{2\pi A'}\delta(x-x_0)\int_0^{2\pi} u[D(y_0,z_0,\boldsymbol{\phi})-v]Q(\gamma,\mu,t)d\gamma. \tag{63b}$$

Besides the point source, which is the most effective source in room-acoustic simulations, line sources and plane sources can also be treated by the one-dimensional transport equation model. For a line source at $x=x_0$, $y=y_0$, which spans from z_0 to z_1, the source term is written as $Q(\gamma,\mu,t)\delta(x-x_0)\delta(y-y_0)\chi_{[z_0,z_1]}(z)$, where χ is the indicator function,

$$\chi_{[B]}(x)=1 \quad \text{if } x\in B,$$

$$\chi_{[B]}(x)=0 \quad \text{if } x\notin B. \tag{64}$$

Q_i immediately becomes

$$Q_1 = \frac{1}{2\pi A'}\delta(x-x_0)(z_1-z_0)\int_0^{2\pi} Q(\gamma,\mu,t)d\gamma, \tag{65a}$$

$$Q_2 = \frac{1}{2\pi A'}\delta(x-x_0)\times\int_0^{2\pi} Q(\gamma,\mu,t)\int_{z_0}^{z_1} u[D(y_0,z,\boldsymbol{\phi})-v]dzd\gamma. \tag{65b}$$

In the same fashion, the source term for a plane source at $x=x_0$ is $Q(\gamma,\mu,t)\delta(x-x_0)$. Q_i are written as

$$Q_1 = \frac{1}{2\pi}\delta(x-x_0)\int_0^{2\pi} Q(\gamma,\mu,t)d\gamma, \tag{66a}$$

$$Q_2 = \frac{1}{2\pi A'}\delta(x-x_0)\times\int_0^{2\pi} Q(\gamma,\mu,t)\int_A u[D(y,z,\boldsymbol{\phi})-v]dydzd\gamma. \tag{66b}$$

For one-group model, only Q_1 is needed.

2. Furnished rooms

In furnished rooms (sometimes also called fitted rooms[30]), the interior contains noticeable objects (fittings), e.g., machines, chairs, and desks. Some factories, classrooms, and offices are studied as furnished rooms. In these cases, the theory for empty rooms no longer holds—the fittings inside the room need to be considered. In general, the sound field in a furnished room is complex due to different locations, absorption, and scattering coefficients of objects inside the room. Our goal is to model a simple case where the objects inside the room have more or less the same absorption and scattering coefficients, and the positions of

these scattering objects can be statistically described by the mean free path between them, which can be obtained by a best-fit approach.[31] To further simplify the problem, the scattering of the sound by the fittings is modeled as a uniform isotropic scattering. For furnished rooms, the three-dimensional transport equation is

$$\frac{1}{c}\frac{\partial \psi}{\partial t}(\boldsymbol{r},\boldsymbol{\Omega},t)+\boldsymbol{\Omega}\cdot\nabla\psi(\boldsymbol{r},\boldsymbol{\Omega},t)+(M+\sigma_T)\psi(\boldsymbol{r},\boldsymbol{\Omega},t)$$
$$=\frac{\sigma_S}{4\pi}\int_{4\pi}\psi(\boldsymbol{r},\boldsymbol{\Omega}',t)d\Omega'+\frac{Q(\boldsymbol{r},t)}{4\pi},$$
$$0<x<L,\quad (y,z)\in A, \tag{67}$$

where $\sigma_T=\sigma_S+\sigma_A$, and σ_S and σ_A are the so-called scattering and absorption coefficients for the fittings, respectively. It can be shown that[13]

$$\sigma_T=\frac{1}{\lambda'}, \tag{68a}$$

$$\sigma_A=\frac{-\ln(1-\alpha_f)}{\lambda'}, \tag{68b}$$

where λ' is the mean free path between the scattering objects in the room, and α_f is the sound energy absorption coefficient of the fittings. A similar equation is documented in Ref. 32, with the absorption term being

$$\sigma_A=\frac{\alpha_f}{\lambda'}. \tag{69}$$

This difference has been explained in Refs. 13 and 33.

Repeating the same analysis for the empty room case, the one-dimensional transport equation model for the furnished rooms can be obtained. For example, the one-group model is written as

$$\frac{1}{c}\frac{\partial \psi_1}{\partial t}+\mu\frac{\partial \psi_1}{\partial x}+(M+\sigma_T)\psi_1+\sqrt{1-\mu^2}a_{11}\psi_1$$
$$=\frac{\sigma_S}{2}\int_{-1}^{1}\psi_1(\mu')d\mu'+\frac{2sR}{\pi}\sqrt{1-\mu^2}b_{11}$$
$$\times\int_{-1}^{1}\sqrt{1-\mu'^2}\psi_1(\mu')d\mu'+Q_1. \tag{70}$$

III. CONCLUSIONS

This paper proposes a set of coupled one-dimensional transport equations, which are derived from the exact three-dimensional transport equation, to predict the steady-state and time-dependent sound fields in elongated spaces.

The aim of this work is to develop an efficient mathematical model for predicting long room acoustics by concentrating on the long dimension and "eliminating" the other two dimensions. It is hoped that, by using this one-dimensional model, the calculation load can be significantly lessened with little loss of accuracy.

The "journey" from the three-dimensional transport equation to the one-dimensional transport equations lies in the method of weighted residuals, by which the sound angular flux is essentially divided into two parts. One is the sound energy propagation in the long dimension, while the other is a set of predetermined basis functions of cross-sectional parameters.

The one-dimensional one- and two-group transport equation models developed in this paper have simple formats. They differ from each other by having one one-dimensional transport equation and two one-dimensional transport equations, respectively. The one-group transport equation model essentially assumes that the energy flux has weak dependence on the cross-sectional spatial and angular variables. Therefore, it is likely to be suitable only for cases where a light-damping condition is satisfied. The two-group transport equation model improves the accuracy of the one-group model by taking the dependence on the cross-sectional variables into account. However, the two-group model is more complex. A simple numerical example has been carried out for sound propagation from an omnidirectional source to a free space. The result suggests that the two-group model is indeed more accurate.

This paper has shown that the one-dimensional models are able to simulate different types of sources, with various directivities. Fittings in the room can also be modeled as interior scattering objects. Thus, the one-dimensional models are applicable for modeling empty rooms and fitted rooms.

ACKNOWLEDGMENTS

The authors would like to thank Professor H. Kuttruff, Professor M. M. R. Williams, and Professor Roberto D. M. Garcia for helpful discussions.

APPENDIX: DERIVATION OF THE ONE–DIMENSIONAL TRANSPORT EQUATION MODEL

This appendix elaborates on the derivation of the one-dimensional transport equation model, i.e., Eq. (27). Applying Eq. (22) to Eq. (23) first, using the identity

$$\beta_i\boldsymbol{\phi}\cdot\nabla\psi=\boldsymbol{\phi}\cdot\nabla(\beta_i\psi)-\psi\boldsymbol{\phi}\cdot\nabla\beta_i$$
$$=\nabla\cdot(\beta_i\psi\boldsymbol{\phi})-\beta_i\psi\nabla\cdot\boldsymbol{\phi}-\psi\boldsymbol{\phi}\cdot\nabla\beta_i \tag{A1}$$

and the divergence theorem to Eq. (23), yields

$$F_i=-\frac{\sqrt{1-\mu^2}}{2\pi A'}\left(\int_{\partial A}\int_0^{2\pi}\boldsymbol{\phi}\cdot\boldsymbol{n}\beta_i\psi d\gamma ds'\right.$$
$$\left.-\int_A\int_0^{2\pi}\psi\boldsymbol{\phi}\cdot\nabla\beta_i d\gamma dydz\right), \tag{A2}$$

where

$$F_i=\frac{1}{c}\frac{\partial \psi_i}{\partial t}+\mu\frac{\partial \psi_i}{\partial x}+M\psi_i-Q_i. \tag{A3}$$

By splitting the integral over γ into two parts: $\boldsymbol{\phi}\cdot\boldsymbol{n}<0$ and $\boldsymbol{\phi}\cdot\boldsymbol{n}>0$, substitution of Eq. (3) into Eq. (A2) yields

$$F_i = -\frac{\sqrt{1-\mu^2}}{2\pi A'}\left\{\int_{\partial A}\int_{\boldsymbol{\phi}\cdot\boldsymbol{n}>0}\boldsymbol{\phi}\cdot\boldsymbol{n}\beta_i\psi d\gamma ds' + \int_{\partial A}\int_{\boldsymbol{\phi}\cdot\boldsymbol{n}<0}\boldsymbol{\phi}\cdot\boldsymbol{n}\beta_i R\left[(1-s)\psi(\hat{\boldsymbol{\Omega}}) + \frac{s}{\pi}\int_{\boldsymbol{\Omega}'\cdot\boldsymbol{n}>0}\boldsymbol{\Omega}'\cdot\boldsymbol{n}\psi(\boldsymbol{\Omega}')d\Omega'\right]d\gamma ds' - \int_A\int_0^{2\pi}\psi\boldsymbol{\phi}\cdot\nabla\beta_i d\gamma dy dz\right\}. \quad (A4)$$

From Eqs. (10), (11), and (40b),

$$\int_{\boldsymbol{\phi}\cdot\boldsymbol{n}<0}\boldsymbol{\phi}\cdot\boldsymbol{n}\psi(\hat{\boldsymbol{\Omega}})d\gamma = -\int_{\hat{\boldsymbol{\phi}}\cdot\boldsymbol{n}>0}\hat{\boldsymbol{\phi}}\cdot\boldsymbol{n}\psi(\hat{\boldsymbol{\Omega}})d\hat{\gamma} = -\int_{\boldsymbol{\phi}\cdot\boldsymbol{n}>0}\boldsymbol{\phi}\cdot\boldsymbol{n}\psi(\boldsymbol{\Omega})d\gamma, \quad (A5)$$

and

$$\int_{\boldsymbol{\phi}\cdot\boldsymbol{n}<0}\boldsymbol{\phi}\cdot\boldsymbol{n}u(D-v)\psi(\hat{\boldsymbol{\Omega}})d\gamma = 0 - uv\int_{\boldsymbol{\phi}\cdot\boldsymbol{n}<0}\boldsymbol{\phi}\cdot\boldsymbol{n}\psi(\hat{\boldsymbol{\Omega}})d\gamma = uv\int_{\boldsymbol{\phi}\cdot\boldsymbol{n}>0}\boldsymbol{\phi}\cdot\boldsymbol{n}\psi(\boldsymbol{\Omega})d\gamma. \quad (A6)$$

Substitution of Eqs. (44), (45), (A5), and (A6) into Eq. (A4) yields

$$F_1 = -\frac{\sqrt{1-\mu^2}}{2\pi A'}\left\{[1-R(1-s)]\int_{\partial A}\int_{\boldsymbol{\phi}\cdot\boldsymbol{n}>0}\boldsymbol{\phi}\cdot\boldsymbol{n}\psi d\gamma ds' + \frac{Rs}{\pi}\int_{\partial A}\int_{\boldsymbol{\phi}\cdot\boldsymbol{n}<0}\boldsymbol{\phi}\cdot\boldsymbol{n}\int_{\boldsymbol{\Omega}'\cdot\boldsymbol{n}>0}\boldsymbol{\Omega}'\cdot\boldsymbol{n}\psi(\boldsymbol{\Omega}')d\Omega' d\gamma ds'\right\} \quad (A7)$$

and

$$F_2 = -\frac{\sqrt{1-\mu^2}}{2\pi A'}\left[\int_{\partial A}\int_{\boldsymbol{\phi}\cdot\boldsymbol{n}>0}\boldsymbol{\phi}\cdot\boldsymbol{n}\beta_2\psi d\gamma ds' + R(1-s)uv\times\int_{\partial A}\int_{\boldsymbol{\phi}\cdot\boldsymbol{n}>0}\boldsymbol{\phi}\cdot\boldsymbol{n}\psi d\gamma ds' + \frac{Rs}{\pi}\int_{\partial A}\int_{\boldsymbol{\phi}\cdot\boldsymbol{n}<0}\boldsymbol{\phi}\cdot\boldsymbol{n}\beta_2\times\int_{\boldsymbol{\Omega}'\cdot\boldsymbol{n}>0}\boldsymbol{\Omega}'\cdot\boldsymbol{n}\psi(\boldsymbol{\Omega}')d\Omega' d\gamma ds' - \int_A\int_0^{2\pi}\psi\boldsymbol{\phi}\cdot\nabla\beta_2 d\gamma dy dz\right]. \quad (A8)$$

For F_i where $i>2$, similar equations can be derived if α_i and β_i are known. This is, however, not discussed here.

Moreover, by recognizing that

$$\int_{\boldsymbol{\Omega}'\cdot\boldsymbol{n}>0}(\boldsymbol{\Omega}'\cdot\boldsymbol{n})(\cdot)d\Omega' = \int_{\boldsymbol{\phi}'\cdot\boldsymbol{n}>0}\boldsymbol{\phi}'\cdot\boldsymbol{n}\int_{-1}^{1}\sqrt{1-\mu'^2}(\cdot)d\mu' d\gamma' \quad (A9)$$

and employing Eq. (22),

$$\int_{\boldsymbol{\phi}\cdot\boldsymbol{n}<0}\boldsymbol{\phi}\cdot\boldsymbol{n}\beta_i\left[\int_{\boldsymbol{\Omega}'\cdot\boldsymbol{n}>0}\boldsymbol{\Omega}'\cdot\boldsymbol{n}\psi(\boldsymbol{\Omega}')d\Omega'\right]d\gamma = \int_{\boldsymbol{\phi}\cdot\boldsymbol{n}<0}\boldsymbol{\phi}\cdot\boldsymbol{n}\beta_i \times\left[\int_{\boldsymbol{\phi}'\cdot\boldsymbol{n}>0}\boldsymbol{\phi}'\cdot\boldsymbol{n}\left(\int_{-1}^{1}\sqrt{1-\mu'^2}\psi d\mu'\right)d\gamma'\right]d\gamma = -\sum_{j=1}^{N}\left(\int_{-1}^{1}\sqrt{1-\mu'^2}\psi_j d\mu'\int_{\boldsymbol{\phi}\cdot\boldsymbol{n}<0}|\boldsymbol{\phi}\cdot\boldsymbol{n}|\beta_i d\gamma \times\int_{\boldsymbol{\phi}\cdot\boldsymbol{n}>0}\boldsymbol{\phi}\cdot\boldsymbol{n}\alpha_j d\gamma\right). \quad (A10)$$

Substituting Eq. (A10) into Eqs. (A7) and (A8), the one-dimensional transport model, Eq. (27), is finally obtained.

[1] J. Kang, *Acoustics in Long Spaces: Theory and Design Guide* (Thomas Thelford, London, 2002).
[2] H. Kuttruff, *Room Acoustics*, 4th ed. (Spon, New York, 2000).
[3] H. Kuttruff, "Stationare schallausbreitung in langraumen (Steady-state sound transmission in elongated enclosures)," Acustica **69**, 53–62 (1989).
[4] J. Kang, "Reverberation in rectangular long enclosures with geometrically reflecting boundaries," Acust. Acta Acust. **82**, 509–516 (1996).
[5] K. M. Li and K. K. Lu, "Propagation of sound in long enclosures," J. Acoust. Soc. Am. **116**, 2759–2770 (2004).
[6] A. M. Ondet and J. L. Barbry, "Modeling of sound propagation in fitted workshops using ray tracing," J. Acoust. Soc. Am. **85**, 787–796 (1989).
[7] L. Yang and B. M. Shield, "The prediction of speech intelligibility in underground stations of rectangular cross section," J. Acoust. Soc. Am. **109**, 266–273 (2001).
[8] M. M. Carroll and C. F. Chien, "Decay of reverberant sound in a spherical enclosure," J. Acoust. Soc. Am. **62**, 1442–1446 (1977).
[9] J. Kang, "Reverberation in rectangular long enclosures with diffusely reflecting boundaries," Acust. Acta Acust. **88**, 77–87 (2002).
[10] J. Picaut, L. Simon, and J. D. Polack, "A mathematical model of diffuse sound field based on a diffusion equation," Acust. Acta Acust. **83**, 614621 (1997).
[11] V. Valeau, J. Picaut, and M. Hodgson, "On the use of a diffusion equation for room-acoustic prediction," J. Acoust. Soc. Am. **119**, 1504–1513 (2006).
[12] Y. Jing and N. Xiang, "A modified diffusion equation for room-acoustic predication," J. Acoust. Soc. Am. **121**, 3284–3287 (2007).
[13] Y. Jing and N. Xiang, "On boundary conditions for the diffusion equation in room-acoustic prediction: Theory, simulations, and experiments," J. Acoust. Soc. Am. **123**, 145–153 (2008).
[14] S. Siltanen, T. Lokki, S. Kiminki, and L. Savioja, "The room acoustic rendering equation," J. Acoust. Soc. Am. **122**, 1624–1635 (2007).
[15] M. Hodgson, "Evidence of diffuse surface reflections in rooms," J. Acoust. Soc. Am. **89**, 765–771 (1991).
[16] C. Foy, V. Valeau, A. Billon, J. Picaut, and A. Sakout, "An empirical diffusion model for acoustic prediction in rooms with mixed diffuse and specular reflections," Acust. Acta Acust. **95**, 97–105 (2009).
[17] N. Korany, J. Blauert, and O. A. Alim, "Acoustic simulation of rooms with boundaries of partially specular reflectivity," Appl. Acoust. **62**, 875–887 (2001).
[18] T. Le Pollès, J. Picaut, M. Bérengier, and C. Bardos, "Sound field modeling in a street canyon with partially diffusely reflecting boundaries by the transport theory," J. Acoust. Soc. Am. **116**, 2969–2983 (2004).

[19]T. Le Pollès, J. Picaut, S. Colle, M. Bérengier, and C. Bardos, "Sound-field modeling in architectural acoustics by a transport theory: Application to street canyons," Phys. Rev. E **72**, 046609 (2005).
[20]A. K. Prinja and G. C. Ponraning, "A statistical model for transport in a vacuum," Transp. Theory Stat. Phys. **13**, 567–598 (1984).
[21]E. W. Larsen, "A one-dimensional model for three-dimensional transport in a pipe," Transp. Theory Stat. Phys. **13**, 599–614 (1984).
[22]E. W. Larsen, F. Malvagi, and G. C. Pomraning, "One-dimensional models for neutral particle transport in ducts," Nucl. Sci. Eng. **93**, 13–30 (1986).
[23]W. B. Joyce, "Classical-particle description of photons and phonons," Phys. Rev. D **9**, 3234–3256 (1974).
[24]A. Billon, C. Foy, J. Picaut, V. Valeau, and A. Sakout, "Modeling the sound transmission between rooms coupled through partition alls by using a diffusion model," J. Acoust. Soc. Am. **123**, 4261–4271 (2008).
[25]H. Grandin, *Fundamentals of the Finite Element Method* (Waveland Press, Inc., Prospect Heights, IL, 1991).
[26]P. S. Krämer, "Mean free path length for radiating point source in specular reflecting enclosures," Acust. Acta Acust. **83**, 629–634 (1997).
[27]W. J. M. de Kruijf and J. L. Kloosterman, "On the average chord length in reactor physics," Ann. Nucl. Energy **30**, 549–553 (2003).
[28]Y. Jing and N. Xiang, "One-dimensional transport equation models for sound energy propagation in long spaces: Simulations and experiments," J. Acoust. Soc. Am. **127**, 2323–2331 (2010).
[29]A. D. Pierce, *Acoustics: An Introduction to Its Physical Principles and Applications* (Acoustical Society of America, New York, 1981).
[30]V. Valeau, M. Hodgson, and J. Picaut, "A diffusion-based analogy for the prediction of sound fields in fitted rooms," Acust. Acta Acust. **93**, 94–105 (2007).
[31]M. Hodgson, "Effective densities and absorption coefficients of fittings in industrial work-rooms," Acust. Acta Acust. **85**, 108–112 (1999).
[32]H. Kuttruff, "A mathematical model for noise propagation between buildings," J. Sound Vib. **85**, 115–128 (1982).
[33]U. J. Kurze, "Scattering of sound in industrial spaces," J. Sound Vib. **98**, 349–364 (1985).

A.2 Article 2

One-dimensional transport equation models for sound energy propagation in long spaces: Simulations and experiments

Yun Jing[a] and Ning Xiang
Graduate Program in Architectural Acoustics, School of Architecture, Rensselaer Polytechnic Institute, Troy, New York 12180

(Received 8 September 2009; revised 5 January 2010; accepted 7 January 2010)

In this paper, the accuracy and efficiency of the previously discussed one-dimensional transport equation models [Y. Jing *et al.*, J. Acoust. Soc. Am. **127**, 2312–2322 (2010)] are examined both numerically and experimentally. The finite element method is employed to solve the equations. Artificial diffusion is applied in the numerical implementation to suppress oscillations of the solution. The transport equation models are then compared with the ray-tracing based method for different scenarios. In general, they are in good agreement, and the transport equation models are substantially less time consuming. In addition, the two-group model is found to yield more accurate results than the one-group model for the tested cases. Lastly, acoustic experimental results obtained from a 1:10 long room scale-model are used to verify the transport equation models. The results suggest that the transport equation models are able to accurately model the sound field in a long space. © *2010 Acoustical Society of America.* [DOI: 10.1121/1.3303981]

PACS number(s): 43.55.Br, 43.55.Ka [EJS] Pages: 2323–2331

I. INTRODUCTION

This paper verifies the one-dimensional transport equation models in long spaces[1] using both numerical simulations and acoustical experimental results. A companion paper has presented theoretical formulations of a subset of one-dimensional transport equation models for acoustic prediction in long spaces. These models drastically simplify the three-dimensional exact model by reducing five variables to two (three in space, two in angle); thus, they are expected to be less time consuming in comparison with ray-tracing based methods[2] or radiosity based methods[3] when implemented numerically. On the other hand, a simple example of a sound field in free space has demonstrated that these models are fairly good approximations to the exact model.[1] Particularly, since the diffusion equation can be derived as the asymptotic approximation of the transport equation in certain cases,[4,5] the transport equation method will perform significantly better than the diffusion equation model[4,6–9] recently applied in room-acoustics. For example, the transport equation takes the direct sound field into account while the diffusion equation fails to do so; therefore, the diffusion equation is only valid in the late time.[10] The diffusion equation is inherently unsuitable for problems where the absorption involved is high,[11] while the transport equation is much less restricted to this condition. The diffusion equation model assumes diffusely reflecting surface in the enclosure under investigation while the transport equation can handle explicitly partial specular and partial scattering reflections. In addition, solving the present one-dimensional transport equation does not necessarily take much longer time than solving the three-dimensional diffusion equation. This follow-up paper focuses on solving both the one- and two-group transport equation models numerically for different long spaces and compares the results with those obtained with a ray-tracing based method as well as experimental results obtained from a long room scale-model.

This paper is structured as follows: Sec. II briefly revisits the one-dimensional transport equation models for room-acoustic prediction in long spaces and then introduces solution methods used in solving the equations. Section III discusses simulation results obtained using the transport equation models in comparison with the ray-tracing based method. Section IV describes the scale-model experiments and compares the acoustical measurement results with those obtained using the two-group transport equation model. Section V concludes the paper.

II. ONE-DIMENSIONAL TRANSPORT EQUATION MODELS

A. Governing equations

This section briefly reviews the one-dimensional transport equation models for sound propagation in a long enclosure.

Based on the concept of geometrical acoustics, the sound angular flux $\psi(\mathbf{r},\mathbf{\Omega},t)$ everywhere in a long space [with $\mathbf{r}=(x,y,z)$ and x being the longest dimension ranging from 0 to L] is shown to be the solution of a three-dimensional transport equation

$$\frac{1}{c}\frac{\partial\psi}{\partial t}(\mathbf{r},\mathbf{\Omega},t)+\mathbf{\Omega}\cdot\nabla\psi(\mathbf{r},\mathbf{\Omega},t)+M\psi(\mathbf{r},\mathbf{\Omega},t)=\frac{Q(\mathbf{r},t)}{4\pi},\quad 0<x<L\quad (y,z)\in A, \tag{1}$$

with appropriate boundary conditions, where $\mathbf{\Omega}$ is the unit vector in direction of flight, c is the speed of sound, M is the

[a]Author to whom correspondence should be addressed. Electronic mail: jingy@bwh.harvard.edu

atmospheric attenuation constant, Q is a source term, t is the time, and A is the cross section of the long space.

This radiative transport equation has the same form as the one used in the geometrical optic model.[12] Both models assume that waves behave as particles: phonon and photon. The direct solution of this transport equation is the angular flux (sometimes called radiance), which can immediately lead to the sound intensity and sound pressure by applying an integral over all the angles. Mathematically, a similar radiative transport equation can be derived from the wave equation in the high frequency regime by using the Wigner distribution.[13–15] The solution of this transport equation is an energy density in the phase space whose average over wavenumbers provides the spatial distribution of the energy density. However, this model is more mathematically complicated and less understood in room-acoustic community, which has not adopted it for use in room-acoustic predictions.

Using the method of weighted residuals (Galerkin), the angular flux ψ can be approximated by[16]

$$\psi(x,y,z,\mu,\gamma,t) \approx \sum_{j=1}^{N} \alpha_j(y,z,\gamma)\psi_j(x,\mu,t), \tag{2}$$

where α_j are prescribed basis functions, ψ_j are unknown expansion functions, μ and γ are angular variables, and the three-dimensional exact transport equation can be reduced to a coupled set of one-dimensional transport equations. Keeping the first or the first two one-dimensional transport equations leads to the so-called one- and two-group models, respectively. For an omnidirectional point source at (x_0,y_0,z_0), the one-dimensional transport equation model is written as

$$\frac{1}{c}\frac{\partial \psi_i}{\partial t} + \mu\frac{\partial \psi_i}{\partial x} + M\psi_i + \sqrt{1-\mu^2}\sum_{j=1}^{N} a_{ij}\psi_j = \frac{2Rs}{\pi}\sqrt{1-\mu^2}\sum_{j=1}^{N} b_{ij}\int_{-1}^{1}\sqrt{1-\mu'^2}\psi_j(\mu')d\mu' + Q_i, \tag{3}$$

where $N(\text{or } i)=1,2$ for one- and two-groups models, respectively, R is the average energy reflection coefficient, s is the average scattering coefficient,[17] which expresses the energy fraction between nonspecualr and specular reflections, and a_{ij} and b_{ij} are predefined functions associated with the basis functions

$$a_{11} = [1-R(1-s)]\frac{L'}{\pi A'},$$

$$a_{12} = [1-R(1-s)]\left(u - uv\frac{L'}{\pi A'}\right),$$

$$a_{21} = [R(1-s)-1]\frac{uvL'}{\pi A'},$$

$$a_{22} = \frac{u^2v^2L'}{\pi A'} + R(1-s)uv\left(u - \frac{uvL'}{\pi A'}\right), \tag{4}$$

$$b_{ij} = \begin{bmatrix} L'/(\pi A') & u - uvL'/(\pi A') \\ -uvL'/(\pi A') & -uv[u - uvL'/(\pi A')] \end{bmatrix}. \tag{5}$$

Here A' is the area of the cross section, which can be arbitrarily convex (circular, rectangular, etc.), L' is the circumference of the cross section, and u and v are both constants:

$$u = \left[\frac{1}{6\pi A'}\int_{\partial A}\int_{0}^{2\pi} \phi\cdot\boldsymbol{n}(D-v)^3 d\gamma ds'\right]^{-1/2}, \tag{6}$$

$$v = \frac{1}{4\pi A'}\int_{\partial A}\int_{\phi\cdot\boldsymbol{n}>0} \phi\cdot\boldsymbol{n}D^2 d\gamma ds', \tag{7}$$

where ds' denotes an increment of arc length. In this study, only square cross-section is considered as it is representative in room-acoustics. A square with a width of d gives that

$$u \approx 3.25/d, \quad v \approx 0.47d. \tag{8}$$

Lastly, the first two terms of the source functions Q_i are formulated as

$$Q_1 = \frac{Q(t)}{4\pi A'}\delta(x-x_0), \tag{9a}$$

$$Q_2 = \frac{Q(t)}{8\pi^2 A'}\delta(x-x_0) \times \int_0^{2\pi} u[D(y_0,z_0,\phi)-v]d\gamma, \tag{9b}$$

where $Q(t)$ is the sound source power, δ is the Dirac function, and $D(y,z,\phi)$ is the distance from an interior point (x,y,z) to the boundary along the direction $-\phi$ (where ϕ is the corresponding flight direction of γ).

Two types of boundary conditions for the opposing ends of the long enclosure are proposed to take the absorption into account, when the reflections are either diffuse or specular. The specularly reflecting boundary condition is

$$\psi_1(0,\mu,t) = R'\psi_1(0,-\mu,t), \quad 0<\mu\le 1, \tag{10a}$$

$$\psi_1(L,\mu,t) = R''\psi_1(L,-\mu,t), \quad -1\le\mu<0, \tag{10b}$$

$$\psi_2(0,\mu,t) = R'\psi_2(0,-\mu,t), \quad 0<\mu\le 1, \tag{10c}$$

$$\psi_2(L,\mu,t) = R''\psi_2(L,-\mu,t), \quad -1\le\mu<0, \tag{10d}$$

where R' and R'' are the reflection coefficients of the two ends, respectively.

The diffusely reflecting boundary conditions as follows:

$$\psi_1(0,\mu,t) = 2R'\int_{-1}^{0}(-\mu')\psi_1(0,\mu',t)d\mu', \quad 0<\mu\le 1, \tag{11a}$$

$$\psi_1(L,\mu,t) = 2R''\int_{0}^{1}\mu'\psi_1(0,\mu',t)d\mu', \quad -1\le\mu<0, \tag{11b}$$

$$\psi_2(0,\mu,t) = \frac{R'u^2}{2\pi^2 A'}\left[\int_A \left(\int_0^{2\pi} Dd\gamma\right)^2 dydz - 4\pi^2 v^2 A'\right] \times \int_{-1}^{0} -\mu'\psi_2(0,\mu',t)d\mu', \quad 0 < \mu \le 1, \tag{11c}$$

$$\psi_2(L,\mu,t) = \frac{R''u^2}{2\pi^2 A'}\left[\int_A \left(\int_0^{2\pi} Dd\gamma\right)^2 dydz - 4\pi^2 v^2 A'\right] \times \int_{0}^{1} \mu'\psi_2(0,\mu',t)d\mu', \quad -1 \le \mu < 0. \tag{11d}$$

Note for the diffusely reflecting boundary condition since

$$\frac{R'u^2}{2\pi^2 A'}\left[\int_A \left(\int_0^{2\pi} Dd\gamma\right)^2 dydz - 4\pi^2 v^2 A'\right] \tag{12}$$

is usually very small, the present numerical simulations assume it to be zero. Therefore, Eqs. (11c) and (11d) become

$$\psi_2(0,\mu,t) \approx 0, \quad 0 < \mu \le 1, \tag{13a}$$

$$\psi_2(L,\mu,t) \approx 0, \quad -1 \le \mu < 0. \tag{13b}$$

A linear combination of these two boundary condition types in terms of the absorption and scattering coefficients can be used for partially diffuse reflection. However, for simplification, this study only considers purely specular or diffuse reflections.

The sound pressure level is of the most concern and can be written as

$$L_p(x,y,z,t) = 10\log\left(\frac{I(x,y,z,t)\rho c}{P_{\text{ref}}^2}\right), \tag{14}$$

where

$$I(x,y,z,t) = \int_0^{2\pi}\int_{-1}^{1} \psi d\mu d\gamma \tag{15}$$

is the magnitude of the sound intensity, ρ is the air density, and $P_{\text{ref}}=2\times10^{-5}$ Pa is the pressure reference.

The transport equation models described above will be most accurate when the enclosure considered is sufficiently long (or narrow), as the unknown functions $\psi_j(x,\mu,t)$ imply that the sound energy flux is weakly dependent on y, z, and γ. The limits of aspect ratios (correlated dimensions) where this theory can be applied should be determined on a case-by-case basis in light of the desirable accuracy. However, in this study, the ratio between the length and width (or height) is always larger than 8, and good accuracy has been obtained.

B. Solution method

The one-dimensional transport equation model, which consists of integropartial differential equations, can be solved through the discrete ordinate method.[16] This study utilizes a finite element modeling software to generate the mesh in the domain using the Galerkin method and solve the equations. The spatial x and angular μ variables are discretized (see Fig. 1). Lagrange-quadratic and Lagrange-linear elements are used (basis functions in the finite element implementation are either linear or quadratic on each mesh interval). Their suitability will be discussed. The mesh condition can be found in the convergence study (Sec. III).

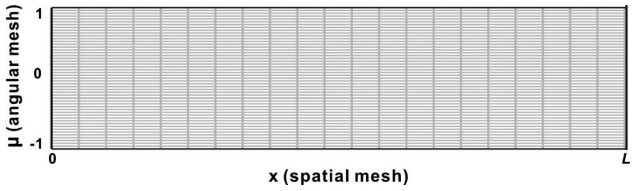

FIG. 1. Meshes for the finite element modeling in the spatial and angular domains.

When solving the steady-state transport equation numerically, artificial oscillations arise, primarily due to two reasons: (1) the equation is convection dominated and (2) the point source term in Eq. (3) introduces a discontinuity/singularity, which cannot be well resolved by the mesh. This will cause an initial disturbance that propagates through the computational domain. Refining the mesh resolution does not reduce the numerical oscillations since the discontinuity still exists and there is no diffusion term in the equation. Also it will be overly demanding of computing resources. Therefore, the anisotropic diffusion technology[18–20] is employed to suppress the oscillations and guarantee reasonable calculation time. The following simple example will briefly explain this. For more information, the reader is referred to Refs. 18–20. Assuming a convection-diffusion transport equation (a parabolic partial differential equation),

$$\frac{\partial u'}{\partial t} + \varepsilon\nabla u' = \nabla(\tau\nabla u'). \tag{16}$$

The Péclet number (Pe)[18–20] is defined as a function of the diffusion coefficient τ, convection function ε, and the mesh element size h,

$$\text{Pe} = \frac{\|\varepsilon\|h}{2\tau}. \tag{17}$$

Since the finite element discretization method used is the Galerkin method, solving such a transport equation becomes unstable when the Péclet number (Pe) is larger than 1. Notice that, in the acoustic transport equation [Eq. (3)], there is no diffusion term, implying that the Péclet number is always larger than 1.

By adding an artificial diffusion term τ_{art}, it is possible to make the Péclet number smaller than 1. The convection term ε is a vector, and anisotropic artificial diffusion adds diffusion only in the direction of the streamline. That is, there is no diffusion added in the direction orthogonal to ε. We now have

$$\tau_{\text{art}} = \frac{\varrho h\varepsilon_i\varepsilon_j}{\|\varepsilon\|}, \quad \text{Pe} = \frac{\|\varepsilon\|h}{2(\tau+\tau_{\text{art}})}, \tag{18}$$

where ϱ is a constant and ε_i and ε_j are components of ε. In this way, the Péclet number measured in the streamline di-

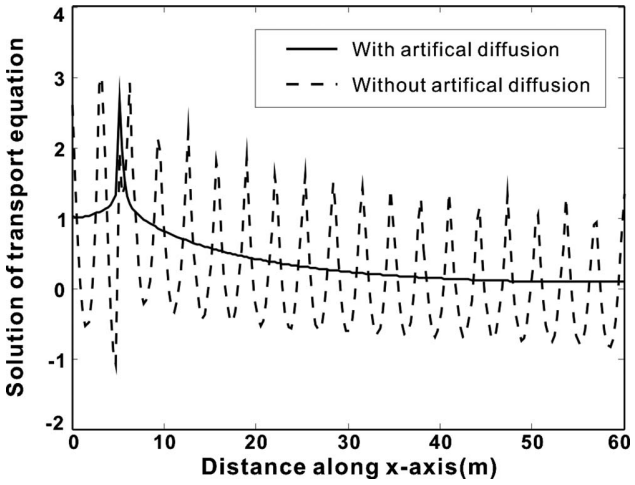

FIG. 2. Comparison of the solution ψ_1 with and without the artificial diffusion.

rection does not exceed 1, given that the constant ϱ is carefully chosen. In the present acoustic transport equation $\varepsilon=[\mu;0]$ (no derivative in the μ-direction), and ϱ is chosen as 0.25. Therefore, to each coupled transport equation, a diffusion term

$$\frac{\varrho h\mu^2}{\|\varepsilon\|}\frac{\partial^2\psi_i}{\partial x^2} \tag{19}$$

is added. Figure 2 shows the comparison between the results with and without artificial diffusion. The artificial diffusion indeed significantly reduces the numerical oscillations. Section III A 1 will discuss the validity of the solution.

When solving the time-dependent transport equation, the interpolating polynomial used in the time-stepping method is the second-order backward differentiation formula.[21] Introducing anisotropic diffusion to suppress oscillations turns out to produce noticeable numerical damping. Therefore, the initial condition should be defined so that it is continuous across the spatial domain, in order to minimize numerical oscillations. An initial condition is used with the Gaussian form

$$\psi(x,y,z,\mu,\gamma,0)=\delta(y-y_0)\,\delta(z-z_0)e^{-((x-x_0)^2/c_0)}, \tag{20}$$

where c_0 controls the width of the Gaussian distribution. Although c_0 should be a frequency dependent parameter, it is chosen as 1.0 in this study for simplicity. It is also found that for smaller c_0, the mesh needs to be denser for obtaining stable numerical results.

Note that in the present model, a single calculation throughout the domain generates the solution at all locations in the volume, which is fundamentally different from the ray-tracing based method where receiver location(s) usually need to be prescribed.

III. NUMERICAL RESULTS

A. Steady-state case

1. Verifications

This section discusses verifications of the present solution method. Same as in Ref. 16, where the study is about neutral particle transport, a circular duct with radius 1 m and length 50 m is tested. The boundaries are all diffusely reflecting. Sound particles enter the duct through one end ($x=0$) of the duct in an isotropic way and leave the duct through the other end which is completely open. The reflection probability at $x=0$ is defined as[16]

$$\hat{R}=\frac{\int_0^1 \mu\psi_1(0,-\mu)d\mu}{\int_0^1 \mu\psi_1(0,\mu)d\mu}. \tag{21}$$

The one-dimensional transport equations for steady-state are solved where the time t is neglected. Numerical results given are from a mesh resolution of 100 angular points and 200 spatial points. Calculation time is around 10 s for the one-group model and 40 s for the two-group model on a current laptop personal computer. The present results are compared with the results from Ref. 16 in Table I, showing good agreements.

TABLE I. Comparison between the present numerical results with the ones in Ref. 16: The probability of reflection for a circular duct with isotropic incidence.

α	$N=1$	$N=1$ [a]	Reflection probability $N=2$	$N=2$ [a]
0.1	0.018	0.018	0.0255	0.0256
0.2	0.038	0.038	0.0539	0.0541
0.3	0.062	0.061	0.0859	0.0862
0.4	0.089	0.089	0.1225	0.1229
0.5	0.123	0.122	0.1652	0.1656
0.6	0.164	0.164	0.2165	0.2170
0.7	0.219	0.218	0.2808	0.2814
0.8	0.296	0.295	0.3671	0.3677
0.9	0.423	0.423	0.5008	0.5014
0.99	0.751	0.751	0.8024	0.8027

[a]From Ref. 16.

2. Convergence study

The goal of this section is to first study the convergence condition when numerically solving the steady-state one-dimensional transport equation models and then to briefly compare the transport equation models with the ray-tracing based method, i.e., the solution of the three-dimensional transport equation. This section only discusses the two-group model since it is expected to be more accurate based on the previous discussion.[1] For steady-state transport equation models, the time variable t is simply discarded. An imaginary long room with dimensions $80\times4\times4$ m^3 is studied. The scattering coefficient is 0.8. The two ends are considered to be specularly reflecting. The absorption coefficient for all surfaces is 0.5. An omnidirectional source is located at (40, 2, 2) m with a sound power of 0.01 W. Here, numerical simulations only involve Lagrange-quadratic elements and observe the sound pressure level at position (60, 2, 2) m for different mesh resolutions. Note that the solution given by the ray-tracing method is 68.3 dB, and the calculation time is more than 5 min for obtaining well converged results. Table II lists the numerical results and suggests that the result in-

TABLE II. Sound pressure level prediction with varying mesh resolutions for a long room.

Spatial point number	Angular point number	Sound pressure level (dB)	Calculation time (s)
50	20	68.38	1
50	50	68.55	4
50	100	68.62	9
100	20	68.20	3
100	50	68.37	8
100	100	68.44	17
200	20	68.11	6
200	50	68.29	15
200	100	68.36	35
400	20	68.07	9
400	50	68.24	31
400	100	68.32	72

deed converges to a finite value as either the spatial or angular resolution increases. In addition, the difference between each prediction is within a tolerable range, which indicates that for predicting sound pressure level, a coarse mesh can be used for solving the one-dimensional two-group transport equation model. The most accurate result (68.32 dB) naturally occurs using the finest mesh. This agrees well with the ray-tracing result.

3. Comparison with ray-tracing simulations

This section compares numerical results from the present transport equation model with the ones from the ray-tracing based method implemented by a commercially available software CATT-acoustics®, for two representative scenarios. A long room with dimensions $60\times6\times6$ m^3 is modeled. An omnidirectional sound source is located at (5, 3, 3) m with sound power of 0.01 W. The receivers are along the line $y=z=3$ m. For the first case, the absorption coefficient is uniform and is 0.05, while in the second case, it is 0.5. The scattering coefficient for all side walls in the first case is 0.9 and 1.0 in the second case. The two end walls are diffusely reflecting. The number of rays for each ray-tracing is 500 000. The truncation time is long enough so that the sound energy decays to a negligible amount. When solving the transport equation, 10 000 mesh elements are constructed. Figures 3 and 4 show the sound pressure level distribution along the x-axis across the center of the long room. The following observations are worth discussing.

(1) For both examples, the two-group model agrees fairly well with the ray-tracing simulation, while the one-group model agrees less well, especially when the receivers are far away from the source, and the absorption involved is high. This observation is consistent with the conclusion in Larsen's paper.[16]
(2) For low absorption case, the maximum deviation of the one-group model from the ray-tracing simulation is around 2.0 dB, which is still acceptable. This suggests that, for stationary sound field predictions in weakly damping long rooms, both one- and two-group models can be employed. Particularly, if the sound field far away from the source is not of major concern, the one-group model works reasonably well.
(3) In Fig. 4, all the three curves show that the sound pressure level increases slightly when the receiver approaches the end ($x=60$ m). This important characteristic, however, cannot be captured by the diffusion equation model,[22] because the diffusion equation model is not accurate near the boundary.[11]

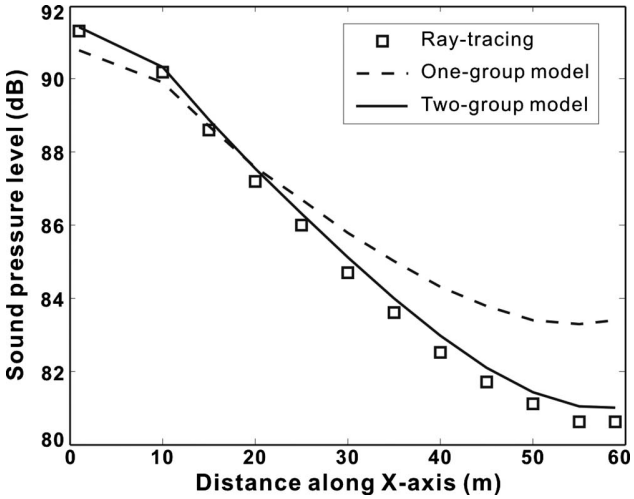

FIG. 3. Comparisons of sound pressure level distributions for a long room ($60\times6\times6$ m^3, uniform absorption coefficient of 0.05, scattering coefficient of 0.9, two end walls are diffusely reflecting) among ray-tracing simulations: one- and two-group models.

B. Time-dependent case

1. Convergence study

This section studies the convergence condition for the time-dependent case in terms of the reverberation time (RT) and early decay time (EDT), again for the two-group model. Compared with the steady-state case, one additional variable, i.e., time t, needs to be counted. The choice of the time step

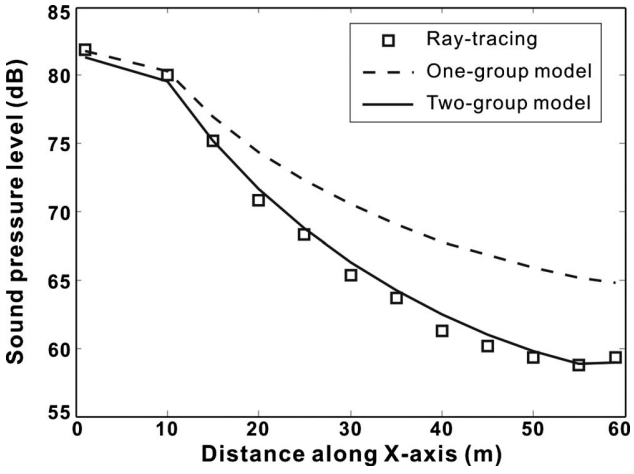

FIG. 4. Comparisons of sound pressure level distributions for a long room ($60\times6\times6$ m^3, uniform absorption coefficient of 0.5, scattering coefficient of 1.0 for all the walls) among ray-tracing simulations: one- and two-group models.

determines the accuracy of the solution and the calculation time, and therefore needs to be carefully examined. For results summarized here, the total number of mesh elements is changed, i.e., the product of both distance and angular point numbers, rather than both distance and angular mesh sizes being varied independently. Two types of mesh elements are considered: quadratic and linear. As anticipated, the former requires longer calculation time. The decay time parameters are found by exciting an impulse in the room using Eq. (20), solving for the sound intensity impulse response from the transport model, and using Schroeder integration[23] to compute for the sound intensity decay function. For calculating the reverberation time, the normalized decay level interval of -5 to -35 dB is used, and for early decay time, from 0 to -10 dB.[24]

The long room model has the same geometry, with dimensions $80\times4\times4$ m^3, as that for the steady-state convergence investigation, the source is also the same, the receiver is located at (20, 2, 2) m, the scattering coefficient for the side walls is 0.8, and the absorption coefficient for all walls is 0.4. For a narrow long room, if the two ends are specularly reflecting and strongly reflective, a randomized ray that happens to shoot exactly perpendicular to the end walls will continue to bounce back and forth between the end walls and create flutter echoes, which makes the energy decay curve irregular/nonexponential. In addition, relatively strong numerical damping has been found for the sound traveling in the direction perpendicular to the end walls ($\mu=\pm1$). Therefore, in the time-dependent case, only diffusely reflecting ends are included in the discussions. The total calculated time length for the transport equation model is 0.8 s, which is much longer than the expected reverberation time. The simulation results given by ray-tracing are 0.38 and 0.35 s for reverberation and early decay times, respectively. The calculation by ray-tracing takes more than 15 min. Figure 5 shows the energy impulse response, energy-time curve, and Schroeder integration curve at the receiver position. The transport equation model simulates the direct sound properly as the energy peak shown approximately at 0.06 s (the time the sound particles take to travel from $x=40$ to 20 m). Table III lists all the results. The first three results are produced with quadratic elements only because linear elements are extremely inaccurate for these three cases. Linear elements are actually also inaccurate for the next three cases, but we keep the results to demonstrate the required element number for linear elements. Table III, along with other related calculations, shows that using a fairly coarse spatial mesh and time step can produce accurate results for both reverberation and early decay times. Linear elements take less time than quadratic elements, and results from the former are reasonably accurate for sufficiently many mesh elements. The key point is that solving the transport equation model produces accurate results in much less time than ray-tracing and the solution at all mesh points throughout the space under investigation is achieved within one calculation run.

2. Comparison with ray-tracing simulations

This section compares numerical results from the present transport equation model with the ray-tracing results for two representative scenarios. A long room with dimension $40\times4\times4$ m^3 is modeled. The source is omnidirectional and is located at (10, 2, 2) m. The receivers are along the line $y=z=2$ m. In the first example, the absorption coefficient 0.2 is assigned uniformly. The scattering coefficient for all the side walls is 0.7. The two end walls are diffusely reflecting, i.e., $s=1.0$. The number of rays is 500 000 for the ray-tracing implementation. 8000 quadratic elements are generated when solving the transport equation. The time step is 0.001 s. Figure 6 shows the reverberation and early decay time trends along the x-axis. The two-group transport model agrees very well with the ray-tracing results, while the one-group model shows noticeable discrepancies with the ray-tracing results for reverberation times. All the models are able to show that reverberation time increases slowly while early decay time increases quickly.[7]

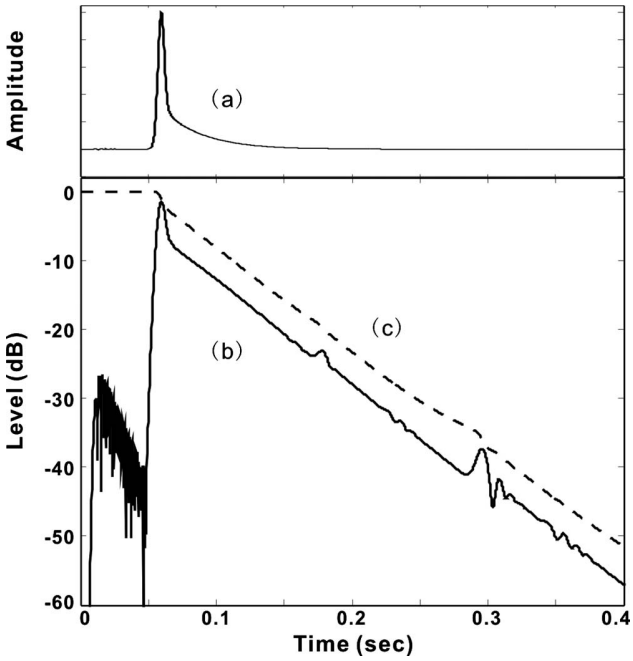

FIG. 5. Time-dependent simulation result: (a) energy decay curve in a long room; (b) logarithmic energy decay; and (c) Schroeder integration curve.

In the second example, the absorption coefficients are 0.4 for the side walls and 0.01 for the two end walls. The scattering coefficient is reduced to 0.5. Figure 7 shows the reverberation and early decay time results. Note that the one-group model is not included in this comparison. The discrepancy between the ray-tracing results and transport equation model results is still sufficiently small. These two cases suggest that the transport equation model, especially the two-group model, is fully capable of predicting sound energy decays in a long space. At least the accuracy of the present model is on the same level as a commercial acoustic prediction software.

IV. EXPERIMENTAL RESULTS

A. Experimental setup

A long room tenth scale-model is built to further assess the accuracy of the transport equation model. The reasons for

TABLE III. Reverberation time and early decay time predictions with varying mesh resolutions and time steps for a long room.

Element No.	Element type	Time step (s)	RT (s)	EDT (s)	Calculation time (s)
1000	Quadratic	0.002	0.404	0.419	19
1000	Quadratic	0.001	0.406	0.419	30
1000	Quadratic	0.0005	0.406	0.418	53
2000	Quadratic	0.002	0.401	0.376	38
2000	Linear	0.002	0.002	0.013	6
2000	Quadratic	0.001	0.402	0.379	61
2000	Linear	0.001	0.001	0.019	18
2000	Quadratic	0.0005	0.403	0.380	105
2000	Linear	0.0005	0.001	0.019	18
5000	Quadratic	0.002	0.401	0.360	99
5000	Linear	0.002	0.391	0.374	17
5000	Quadratic	0.001	0.404	0.362	166
5000	Linear	0.001	0.387	0.376	29
5000	Quadratic	0.0005	0.404	0.360	273
5000	Linear	0.0005	0.387	0.377	52

choosing physical scale modeling are its versatility and easy access.[10,25] The dimensions of the scale-model are $2.4 \times 0.24 \times 0.24$ m^3, which corresponds to $24 \times 2.4 \times 2.4$ m^3 for real size. This scale-model is built of $\frac{3}{8}$ in.-thick hard plywood. The wall surfaces are relatively smooth, only featured with small scale roughness (<0.2 cm in depth). Figure 8 shows a photograph of the scale-model with the top and two ends open. A miniature dodecahedron loudspeaker system used as the sound source is located at (6.1, 1.2, 1.2) m [see Fig. 9(a)]. It is reasonably omnidirectional up to 32 kHz. A $\frac{1}{4}$ in. microphone is used as the receiver to measure the room impulse responses excited by maximal-length sequences of $2^{18}-1$, averaged over ten repetitions. The microphone is moved along the centerline of the scale-model throughout the measurements. Fourteen measurements are conducted with an equidistant separation along the x-axis and are repeated five times to show the repeatability/uncertainty of the experiment. Measurements of the sound field close to the source are avoided since the source directivity has a greater impact on the near field. Neither nitrogen nor air drying is used to compensate for the air attenuation, as the air attenuation can be included in the transport equation model (see Sec. IV B), and the purpose of this measurement is only to verify the present model rather than to model an existing space. (The following discussion will only use real-sized dimensions.)

B. Experimental verifications of the transport equation model

This section aims to verify the transport equation model by comparing the experimental results with the simulation results. As the geometrical-acoustic model works only properly in a high frequency broad-band range, the results at 1–2

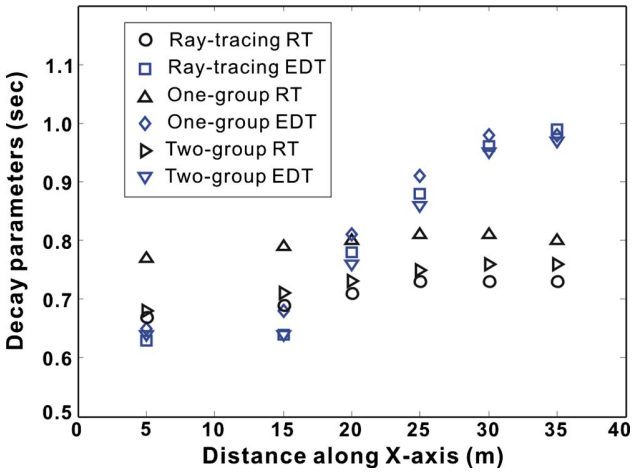

FIG. 6. (Color online) Comparisons of reverberation time and early decay time distributions for a long room ($40 \times 4 \times 4$ m^3, uniform absorption coefficient of 0.2, scattering coefficient of 0.7) among ray-tracing simulations: one- and two-group models.

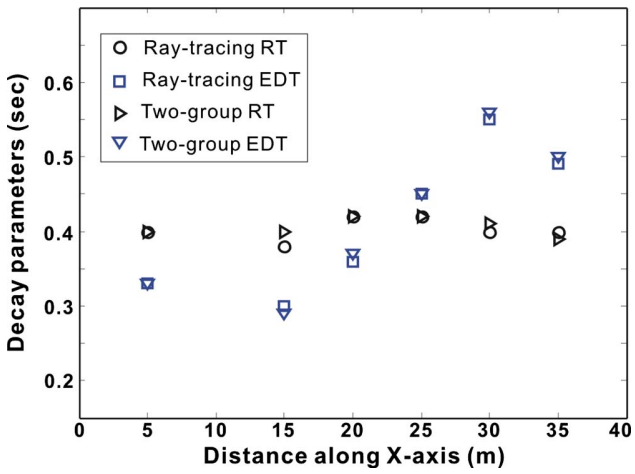

FIG. 7. (Color online) Comparisons of reverberation time and early decay time distributions for a long room ($40 \times 4 \times 4$ m^3, absorption coefficient of 0.4 for the side walls and 0.01 for the end walls, scattering coefficient of 0.5) between ray-tracing simulations and the two-group model.

FIG. 8. (Color online) Photograph of the long room tenth scale-model with the top and two ends open. Bottom left shows the miniature dodecahedron loudspeaker.

kHz octave broadband are chosen for comparison. In lower frequency bands, wave phenomena, e.g., standing waves, are observed, which cannot be modeled by the transport equation model. In the frequency range of interest (1–2 kHz), the absorption coefficient is estimated to be 0.15. The scattering coefficient is difficult to estimate but is expected to be low (as mentioned above, the wall surface is relatively smooth). An average air attenuation constant of 0.00391 Np/m is used for 10–20 kHz for the tenth-scale factor[26] (temperature of 20 °C and humidity of 50%).

This section only considers the two-group model. The reflections at the two ends are set to be completely diffused. Since two ends of the scale-model are relatively smooth, this will introduce a source of error; however, it is expected to be insignificant because the two ends are small compared with the side walls. For both steady-state and time-dependent cases, two simulations with scattering coefficients of 0.1 and 0.3, respectively, are carried out.

Figure 9(b) shows the comparison of sound pressure level distributions. The transport equation model with scattering coefficient of 0.3 agrees well with the experimental results. Most of results show small deviations (<1 dB). The transport equation model with scattering coefficient of 0.1 matches the experimental results less well but the disparity is still tolerable. This implies that the scattering coefficient is indeed low. To further confirm this, the simulated and measured reverberation times will be compared. Figure 10(a) presents a segment of the room impulse responses recorded 4.6 m from the source. Figure 10(b) illustrates the Schroeder curves given by experimental measurement in comparison with the transport equation model with scattering coefficients of 0.1 and 0.3.

Figure 11 shows a detailed comparison of the reverberation time prediction. Both simulation curves agree well with the measurement. Together with the sound pressure level distribution results, it appears that the scattering coefficient is likely to be between 0.1 and 0.3. So far, the experimental comparisons have demonstrated the validity of the one-dimensional transport equation model for a long space.

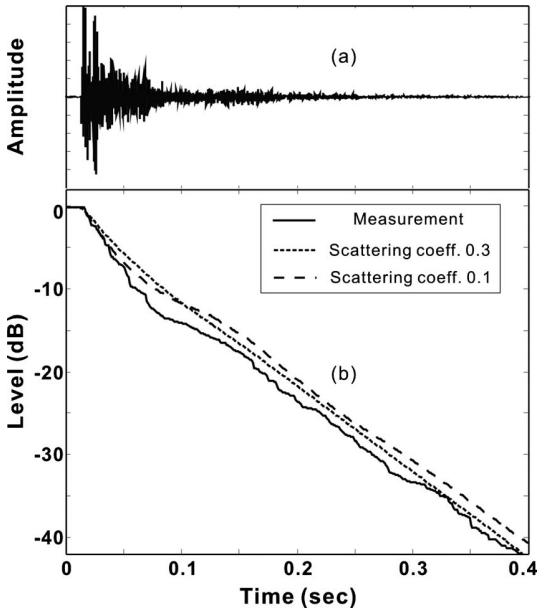

FIG. 10. Comparison between simulated and experimental results in a long room tenth scale-model: (a) segment of a room impulse response measured in a 1:10 long room scale-model; (b) comparison of the Schroeder curve between experiment and simulation. For simulated results, two scattering coefficients of 0.1 and 0.3 are used.

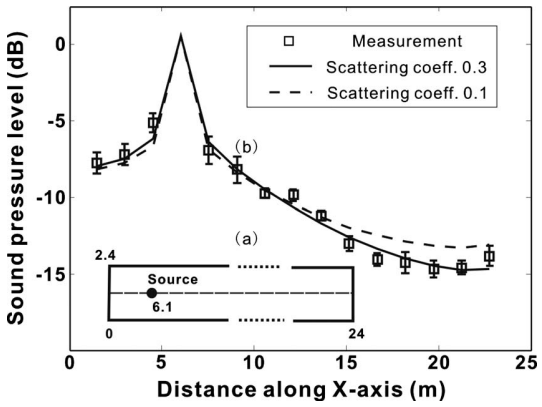

FIG. 9. Comparison between simulated and experimental results in a long room tenth scale-model: (a) top-view of a 1:10 long room scale-model; (b) comparison of sound pressure level distribution between simulated and experimental results. For simulated results, two scattering coefficients of 0.1 and 0.3 are used. The experimental results with error bars are evaluated from five sequentially repetitive measurements.

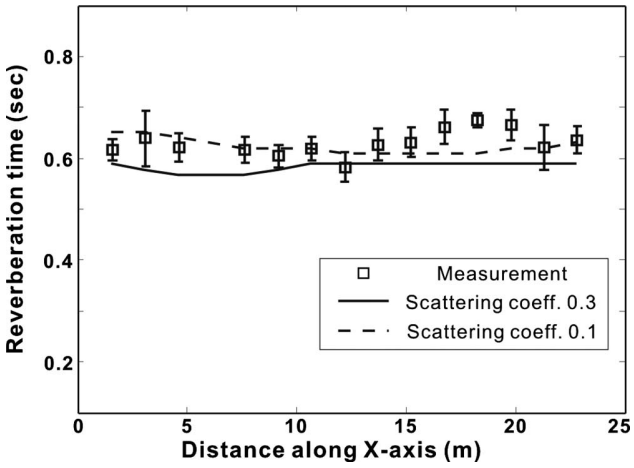

FIG. 11. Comparison of reverberation time between simulated and experimental results in a 1:10 long room scale-model. For simulated results, two scattering coefficients of 0.1 and 0.3 are used. The experimental results with error bars are evaluated from five sequentially repetitive measurements.

V. CONCLUSIONS

This paper has discussed numerical results for a long space room-acoustic model based on one-dimensional transport equations. The transport equation models explicitly handle partial specular, partial scattering, tolerate high overall absorption, and contain direct sound and early reflection portions of sound propagation. Comparisons between the transport equation model and the ray-tracing approach indicate that the solutions given by the one-dimensional transport equation model well approximate the three-dimensional exact solution. Particularly, the two-group model can work properly in a wide range of scenarios. In addition, numerically solving the transport equation models is significantly less time consuming than the ray-tracing approach. Note that the current solution method for the transport equation models is not specifically optimized; therefore, it is possible to speed up the simulation by using advanced technologies.[27] Finally, experimental results from a long room scale-model further validate the transport equation model.

Within the scope of this work, only empty rooms and omnidirectional sound sources are considered. However, these transport equation models can also take interior scattering objects and source directivity into account. These transport equation models can be extended to simulate side walls with nonuniform absorption or scattering coefficients, which makes the model more flexible. This study points out that the transport equation model is more accurate than the diffusion equation model, e.g., near a boundary. Detailed comparisons between the transport and diffusion equation models, which will clarify the relationship of these two models, are also attractive. These issues are expected to be addressed in future work.

ACKNOWLEDGMENTS

The authors would like to thank Professor E. Larson, Professor H. Kuttruff, Profesor W. Siegmann, and Professor J. Wei for their helpful discussions. The authors would also like to thank Mr. Joon Hee Lee and Mr. Gino Pellicano for their assistance in collecting experimental results, and Mr. Robert Bocala and Dr. Phillip Jason White for their critical reviews of the manuscript.

[1]Y. Jing, E. W. Larsen, and N. Xiang, "One-dimensional transport equation models for sound energy propagation in long spaces: Theory," J. Acoust. Soc. Am. **127**, 2312–2322 (2010).
[2]M. Vorländer, "Simulation of the transient and steady-state sound propagation in rooms using a new combined ray-tracing/image-source algorithm," J. Acoust. Soc. Am. **86**, 172–178 (1989).
[3]E. Nosal, M. Hodgson, and I. Ashdown, "Improved algorithms and methods for room sound-field prediction by acoustical radiosity in arbitrary polyhedral rooms," J. Acoust. Soc. Am. **116**, 970–980 (2004).
[4]T. Le Pollès, J. Picaut, M. Bérengier, and C. Bardos, "Sound field modeling in a street canyon with partially diffusely reflecting boundaries by the transport theory," J. Acoust. Soc. Am. **116**, 2969–2983 (2004).
[5]T. Le Pollès, J. Picaut, S. Colle, M. Bérengier, and C. Bardos, "Sound-field modeling in architectural acoustics by a transport theory: Application to street canyons," Phys. Rev. E **72**, 046609 (2005).
[6]J. Picaut, L. Simon, and J. D. Ploack, "A mathematical model of diffuse sound field based on a diffusion equation," Acust. Acta Acust. **83**, 614–621 (1997).
[7]V. Valeau, J. Picaut, and M. Hodgson, "On the use of a diffusion equation for room-acoustic prediction," J. Acoust. Soc. Am. **119**, 1504–1513 (2006).
[8]Y. Jing and N. Xiang, "A modified diffusion equation for room-acoustic predication," J. Acoust. Soc. Am. **121**, 3284–3287 (2007).
[9]Y. Jing and N. Xiang, "On boundary conditions for the diffusion equation in room-acoustic prediction: Theory, simulations, and experiments," J. Acoust. Soc. Am. **123**, 145–153 (2008).
[10]N. Xiang, Y. Jing, and A. Bockman, "Investigation of acoustically coupled enclosures using a diffusion-equation model," J. Acoust. Soc. Am. **126**, 1187–1198 (2009).
[11]P. M. Morse and H. Feshbach, *Methods of Theoretical Physics* (McGraw-Hill, New York, 1953).
[12]A. D. Klose and E. W. Larsen, "Light transport in biological tissue based on the simplified spherical harmonics equations," J. Comput. Phys. **220**, 441–470 (2006).
[13]L. Ryzhik, G. Papanicolaou, and J. B. Keller, "Transport equations for elastic and other waves in random media," Wave Motion **24**, 327–370 (1996).
[14]G. Bal and O. Pinaud, "Accuracy of transport models for waves in random media," Wave Motion **43**, 561–578 (2006).
[15]O. Runborg, "Mathematical models and numerical methods for high frequency waves," Comm. Comp. Phys. **2**, 827–880 (2007).
[16]E. W. Larsen, F. Malvagi, and G. C. Pomraning, "One-dimensional models for neutral particle transport in ducts," Nucl. Sci. Eng. **93**, 13–30 (1986).
[17]M. Vorländer and E. Mommertz, "Definition and measurement of random-incidence scattering coefficients," Appl. Acoust. **60**, 187–199 (2000).
[18]O. C. Zienkiewicz, R. L. Taylor, and P. Nithiarasu, *The Finite Element Method for Fluid Dynamics*, 6th ed. (Elsevier, New York, 2005).
[19]C. Johnson, "Numerical solution of partial differential equations by the finite element method," Acta Applicandae Mathematicae. **18**,184–186 (1987) .
[20]R. Codina, "Comparison of some finite element methods for solving the diffusion-convection-reaction equation," Comput. Methods Appl. Mech. Eng. **156**, 185–210 (1998).
[21]L. F. Shampine, *Numerical Solution of Ordinary Differential Equations* (Chapman and Hall, London, 1994).
[22]J. Picaut, L. Simon, and J. D. Ploack, "Sound field in long rooms with diffusely reflecting boundaries," Appl. Acoust. **56**, 217–240 (1999).
[23]M. R. Schroeder, "New method of measuring reverberation time," J. Acoust. Soc. Am. **37**, 409–412 (1965).
[24]ISO-3382, "Acoustics measurement of room acoustic parameters" (2008).
[25]N. Xiang and J. Blauert, "Binaural scale modeling for auralisation and prediction of acoustics in auditoria," Appl. Acoust. **38**, 267–290 (1993).
[26]ISO-9613, "Acoustics attenuation of sound during propagation outdoors, Part 1: Calculation of the absorption of sound by the atmosphere" (1993).
[27]R. D. M. Garcia and S. Ono, "Improved discrete ordinates calculations for an approximate model of neutral particle transport in ducts," Nucl. Sci. Eng. **133**, 40–54 (1999).